A Numerical Study of Solitonic Boson Stars in General Relativity

Philip Etter

a senior thesis submitted in partial fulfillment

of the requirements for the degree of Bachelor of Arts in Mathematics

at Princeton University

2017

Honor Pledge

I pledge my honor that this paper represents my own work in accordance with University regulations.

Abstract

In the wake of the recent detection of gravitational wave signal GW150914, we investigate whether GW150914 could have been produced by something other than a binary black hole system. Our proposed candidate is a binary system of solitonic boson stars. The choice of solitonic boson stars is due mainly to the structural properties of their ground states, as solitonic boson stars are capable of forming very compact thin-wall ground states which would likely correctly mimic the gravitational signature of the plunge/merger phase of the binary system lifecycle. On the other hand, the question of whether solitonic boson stars could also mimic the gravitational signature of the subsequent ringdown phase is still open. Since there is no hope of replicating the signature if these thin-wall ground states are not stable with respect to small perturbations, our ultimate goal is to study the stability properties of these thin-wall ground states numerically. Pursuing this goal, we have successfully developed numerical methods for both the computation of ground states of boson stars and the simulation of boson stars exposed to a small perturbation from a real scalar eld. Our methods can compute the desired thin-wall ground states of solitonic boson stars, as well as produce a simulation of a perturbed ground state of a mini-boson star. We provide a thorough look at the implementation details of these methods and present our current computational results.

Acknowledgements

I want to start by thanking Professor Frans Pretorius for being my thesis adviser and for taking on someone like me with no background in general relativity or numerical analysis and hardly any physics background. I can con dently and truthfully say that I *thoroughly* enjoyed working with Professor Pretorius, and I appreciate his impressive availability during both the summer I began to learn general relativity and the two semesters I spent working on this project. Attempting research with no prior experience is a daunting task, but I always felt that he would be there to help me if necessary (and it was necessary). I appreciated the sense of direction he gave me while staying laissez-faire and letting me work on what I found interesting. But beyond advising me in this project, Professor Pretorius is just a fantastic person and I'm glad I got the opportunity to learn numerical relativity from him. So, to Professor Pretorius: a sincere thanks for everything you've done for me. I hope we see each other again in the future, and until then, *praise the sun*!

Next, I want to thank my parents for their emotional support. Making it through Princeton wasn't easy, but they were always there for me when things got rough. I want to thank my friends, especially Sam Cabot, for making the stress of the past four years bearable. I want to thank the Princeton math department for letting me learn and work on what I wanted, even if it wasn't math in the traditional sense.

I want to thank Professor Jason Fleischer, who helped introduce me to the amazing world of physics and gave me the opportunity to learn things I otherwise would never have learned. I want to thank Professor Bernard Chazelle, who was, in my opinion, an absolutely phenomenal lecturer with a burning passion for computer science like no one else I've ever

met. Seriously though, everything he teaches is pure gold. It's worth taking his classes solely to experience the quality of his lectures, watch him dance energetically around the chalkboard, and laugh at his jokes. Last but not least, I want to thank Professor Sergiu Klainerman for being my second reader.

Contents

List of Figures

List of Tables

Chapter 1

Background

1.1 Introduction

The recent observation of gravitational waves by the Laser Interferometer Gravitational-Wave Observatory (LIGO) has now spurred renewed academic interest in general relativity. Indeed, there are many reasons why the observations are both remarkably impressive as a feat of engineering and exciting as a prospect for future research in the area. Gravitational waves are generally so minuscule that detecting them even in good conditions is a di cult challenge. As such, the signal GW150914 marks the end of an approximately fty year period in which scientists have attempted to show the existence of gravitational waves and con rm the predictions of general relativity for large scale cosmic events. In fact, the detection of GW150914 is thanks to a multitude of lucky factors which contributed to the loudness of the signal. These include both the proximity of the merger to Earth as well as the scale of the underlying cosmic event.

Because it matches the predictions of numerical relativity, the signal GW150914 is presumed to be the result of a binary merger of two black holes with masses $36^{+5}_{4}M$ and $29^{+4}_{4}M$ with eventual \ringdown" into a rotating Kerr black hole [1]. The goal of our project is to play Devil's advocate with this presumption. In particular, we ask the driving question,

What if the signal GW150914 was not the result of two black holes merging into another black hole?

It is not inconceivable that two properly chosen stellar objects could merge without collapsing to a black hole and still produce a similar signal to GW150914. Our driving motivation for this project is to look at one such candidate, solitonic boson stars, and try to determine whether mimicking the signal GW150914 is feasible with the merger of two solitonic boson stars into a larger solitonic boson star. To explain why solitonic boson stars are the candidate we want to look at, it would be useful to first establish the properties we desire in our potential candidate.

To begin, the gravitational wave signature of the binary merger of two black holes has roughly three primary components:

1. **Inspiral**: As is implied by the name, this part of the signal is the result of the inward spiral of the two merging objects. Since the two objects only interact through gravity during this phase, it is very difficult to distinguish between different stellar using this part of the signal. As the orbit becomes smaller and smaller, the emission of gravitational waves becomes stronger and the objects orbit with increasing speed.

2. **Plunge/Merger**: When the objects pass the last stable orbit, they enter a plunging orbit and afterwards merge with each other. During this phase, the objects begin to interact directly and produce the strongest part of the signal. In order to reproduce this behavior, the candidate object will have to be very compact, since if the objects begin to interact too early, the result will be markedly distinct from the signal produced by the plunge of two black holes.

3. **Ringdown**: After the merger has finished, the resulting black hole begins to oscillate in shape. This process emits gravitational waves and produces a \ringing" in the signal as the oscillation eventually dampens and the object becomes a Kerr (rotating) black hole.

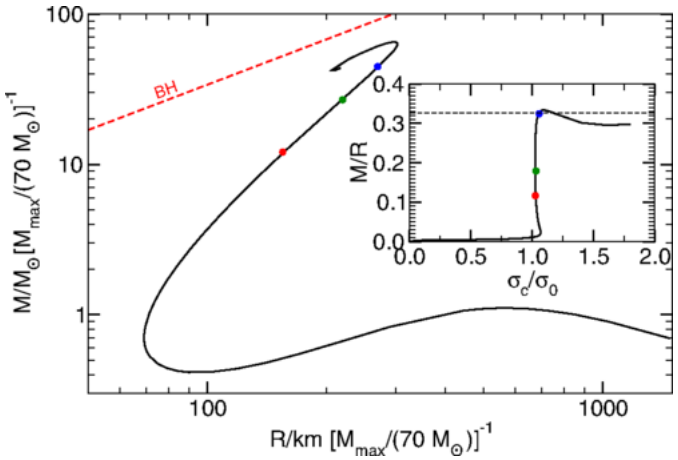

Figure 1.1: Image from [3]. Mass-radius relation for the ground states of solitonic boson star with σ = 0.05m. The inset shows the compactness of the stars as a function of the central scalar eld *j* (r = 0)*j*. The dotted line shows the threshold for black hole formation. The blue marker in the inset indicates a boson star with nearly maximum mass with compactness R/M 3, whereas the green and red markers show boson stars with medium mass and compactness R/M 5.5.

In accordance with the requirements for the plunge/merger, there are ground states of solitonic boson stars which are quite compact and essentially shell-like. These thin-wall ground states consist of a near-vacuum interior and a sharp transition region between interior and exterior. The sharp transition designates a thin shell of mass around the interior vacuum. Thus, it is reasonable to think that it would be quite di cult to distinguish the plunge of two black holes from the plunge of two thin-wall solitonic boson stars by examining the gravitational waves produced.

Therefore, mimicking the signal GW150914 is a problem of replicating the ringdown of binary black holes without our solitonic boson stars collapsing to a black hole. Some results from [3] suggest this approach may perhaps be feasible. In inset of gure 1.1, we can see a plot of compactness versus central eld density. If two boson stars are chosen su ciently below the black hole threshold,[1] the star produced from their merger may also fall beneath this threshold and eventually decay into a thin-wall ground state as it radiates scalar material, \ringing" in the same way as a binary black hole system after merger.

[1] i.e. by the red and green markers in gure 1.1. For reference, the black hole threshold is given by the dotted line

However, our expectation is that this will not be the case { we expect the solitonic boson star will \ring" signi cantly longer as it decays than the binary black hole system. But if the contrary turns out to be true, and the ringdown does resemble that of a binary black hole system, it would be a highly interesting result. Either way, for a solitonic boson star to \ring" in the same way as a binary black hole system, the thin-wall states must also be stable with respect to small perturbations. If not, and a small perturbation causes the thin-wall boson star at the red marker in 1.1 to either collapse to a black hole or explode, then mimicking the signal GW150914 in this manner will certainly not be possible.

This paper is split into three overall chapters. In the rst, we provide background and context relevant to the problem, including a brief overview of general relativity and boson stars. Also, we provide a thorough look at the thin-wall solutions we are interested in, which includes connections to the literature on Q-balls and Q-stars. This is followed by an outline of a relevant work by Choptuik and Hawley concerning the perturbations of mini-boson stars by a real scalar eld, which we will try to replicate for solitonic boson stars instead of mini-boson stars.

Chapter 2 provides details of our work computing these thin-wall ground states numerically. We describe both the algorithm we developed as well as the relevant results and observations of our work. The overarching goal is to provide initial data for the subsequent chapter. Chapter 3 then focuses on the development of a numerical code for perturbing thin-wall ground states, and similarly contains details about the algorithm we use for numerical evolution, followed by tests and results of our code.

1.2 A Quick Review of General Relativity

Before we begin in earnest, a brief note about notation. We will use the common tensor index notation in many general relativity texts such as Carroll, with the convention that Greek indices range from 0 to 3 and Roman indices range from 1 to 3. We will also use the symbol r to denote the covariant derivative.

In essence, general relativity relies upon two principal notions. First is the notion that

the geometry of ambient space is determined by matter and energy, which deform the geometry of spacetime and produce interesting curvature. Second is the notion that the laws of physics should be the same in all coordinate systems (inertial reference frames), which means the underlying equations should be tensorial. Translating this idea into a mathematically precise statement relies heavily on the machinery of di erential geometry. Consider a 4-dimensional Pseudo-Riemannian manifold $(M, g_{\mu\nu})$ where $g_{\mu\nu}$ is a metric of signature $(3,1)$.[2] As mentioned, there is a clearly de ned relationship between the metric $g_{\mu\nu}$ and the matter present on the manifold M. This relationship is explicitly given by Einstein's eld equations, which are commonly written as

$$R_{\mu\nu} \quad \frac{1}{2} g_{\mu\nu} R = \kappa T_{\mu\nu} , \tag{1.1}$$

where $R_{\mu\nu}$ and R denote the Ricci tensor and scalar respectively, quantities which capture the curvature of the manifold M. The quantity $T_{\mu\nu}$ on the right hand side is the stress-energy tensor, which represents the presence of matter in M. We'll return shortly to this important tensor quantity and give it a precise de nition. In the mean time, we examine the rest of the eq. (1.1). The quantity κ is the coupling constant, which determines the strength of gravity. The Ricci tensor $R_{\mu\nu}$ is de ned as a contraction of the Riemann curvature tensor $R^{\sigma}{}_{\mu\rho\nu}$ and can be written explicitly as

$$R_{\mu\nu} = R^{\rho}{}_{\mu\rho\nu} = \partial_{\rho} \ {}^{\rho}{}_{\nu\mu} \quad \partial_{\nu} \ {}^{\rho}{}_{\rho\mu} + \ {}^{\rho}{}_{\rho\lambda} \ {}^{\lambda}{}_{\nu\mu} \quad {}^{\rho}{}_{\nu\lambda} \ {}^{\lambda}{}_{\rho\mu} , \tag{1.2}$$

where ${}^{\rho}{}_{\mu\nu}$ are the Christo el symbols of the metric $g_{\mu\nu}$, given by

$${}^{\sigma}{}_{\mu\nu} = \frac{1}{2} g^{\sigma\rho} \left(\partial_{\mu} g_{\nu\rho} + \partial_{\nu} g_{\rho\mu} \quad \partial_{\rho} g_{\mu\nu} \right) . \tag{1.3}$$

Finally, the Ricci scalar R is de ned as the trace of the Ricci tensor,

$$R \quad g^{\mu\nu} R_{\mu\nu} . \tag{1.4}$$

As one could imagine, the nonlinearity and complexity of Einstein's equations usually makes them too di cult to solve analytically, except in a few special cases where there is a copious amount of symmetry.

[2] or $(1,3)$, depending on convention

The stress-energy tensor $T_{\mu\nu}$ used in eqs. (1.1) depends on the type of object we are trying to model. There are a number of common choices for $T_{\mu\nu}$. For example:

1. $T_{\mu\nu}$ = 0 indicates a $\mathbf{vacuum}$. In contrast with a number of other physical theories, the Einstein eqs. (1.1) actually allow for highly non-trivial dynamics in a vacuum. In the case of a vacuum, the Einstein eqs. (1.1) may be written in the equivalent form

$$R_{\mu\nu} = 0 . \tag{1.5}$$

   The eqs. (1.5) are usually referred to as the Einstein vacuum equations.

2. One can model matter as $\mathbf{dust}$, which is a collection of particles at rest with respect to each other. If we let U^μ be the (constant) four velocity of the particles, then the stress energy tensor is de ned as

$$T^{\mu\nu} \quad \rho U^\mu U^\nu , \tag{1.6}$$

   where $\rho(x^\mu)$ is the energy density at location x^μ in the rest-frame.

3. One can model matter as a $\mathbf{perfect\ fluid}$,

$$T^{\mu\nu} \quad (\rho + p)U^\mu U^\nu + p\eta^{\mu\nu} , \tag{1.7}$$

   where ρ and U^μ are de ned as above, η is the Minkowski metric, and p is the isotropic rest-frame pressure.

There are also other models where the matter in the system is the result of the presence of some eld (e.g. the electromagnetic eld). One can couple matter elds to gravity via the Lagrangian formulation of general relativity. Correspondingly, this gives us another way to specify the stress-energy tensor $T_{\mu\nu}$. The action which gives rise to the dynamics of general relativity is the Einstein-Hilbert action, given by

$$S_{EH} = \int_M \left[\frac{1}{2\kappa}R + L_M\right] \sqrt{-g}\, d^4x , \tag{1.8}$$

where L_M is the Lagrangian of any matter elds present and g is the determinant of the metric $g_{\mu\nu}$. When the action (1.8) is extremized with respect to the inverse metric $g^{\mu\nu}$, we

recover the Einstein eqs. (1.1). If we were to do this computation explicitly, we would see that the stress energy tensor $T_{\mu\nu}$ would take the form

$$T_{\mu\nu} \quad 2\frac{\delta L_M}{\delta g^{\mu\nu}} + g_{\mu\nu} L_M . \tag{1.9}$$

Now suppose, in the absence of gravity (in the Minkowski spacetime), that we have some eld whose dynamics are given by a Lagrangian $L(\ , \partial \ )$ and corresponding action S. The process of coupling a eld to gravity { i.e. adding gravity to the dynamics of { is simply a matter of appropriately de ning the matter Lagrangian L_M in the Einstein Hilbert action S_{EH} (1.8) as $L_M = L$ and taking steps as necessary to ensure that L_M is covariant. The new dynamics of are then given by replacing the nongravitational action S with the gravitational action S_{EH}. Extremizing S_{EH} with respect to $g^{\mu\nu}$ will again give us the Einstein equations, which govern the geometry of the system. On the other hand, extremizing S_{EH} with respect to the eld will give us a set of equations which govern the evolution of the eld . In the scenarios of interest to us, the result for the latter will be the Klein-Gordon equation. Both of these sets of equations are necessary to fully specify the dynamics of this new system with gravitation.

As an illustrative example, let us consider the scalar wave equation on R^{3+1} in a potential V. Here we have a real scalar eld (x^μ) with a nongravitational Lagrangian given by

$$L(\ , \partial \ ) \quad \frac{1}{2}\eta^{\mu\nu}\partial_\mu \ \partial_\nu \quad V(\ ), \tag{1.10}$$

where $\eta^{\mu\nu}$ = diag($1, 1, 1, 1$) is the Minkowski metric. To convince ourselves that the de nition (1.10) makes sense, we note that it corresponds to

$$L(\ , \partial \ ) = \frac{1}{2} - \quad \frac{1}{2}\sum_{i=1}^{3}(\partial_i \ )^2 \quad V(\ ). \tag{1.11}$$

One can identify the distinct terms on the right side of (1.11) as the kinetic energy, gradient energy, and potential energy of , respectively. Moreover, the Lagrangian (1.10) leads to the following Klein-Gordon equation for the dynamics of the system:

$$\eta^{\mu\nu}\partial_\mu\partial_\nu \ = \frac{dV}{d} . \tag{1.12}$$

The objective is now to couple the real field to gravity. As usual when passing from special relativity to general relativity, one begins by replacing the Minkowski metric $\eta_{\mu\nu}$ with the general spacetime metric $g_{\mu\nu}$. The second consideration is to promote the derivatives in the classical Lagrangian to covariant operators, substituting the partial derivative operator ∂_i with the covariant derivative operator ∇_i. The resulting relativistic matter Lagrangian reads

$$\mathcal{L}_M(\ ,\nabla\ ) \qquad \frac{1}{2}g^{\mu\nu}\nabla_\mu\ \nabla_\nu \qquad V(\ ). \tag{1.13}$$

Computing the stress energy tensor for the system from the above Lagrangian can then be done using the expression (1.9). The calculation ultimately yields

$$T_{\mu\nu} = \nabla_\mu\ \nabla_\nu \qquad \frac{1}{2}g_{\mu\nu}\nabla^\alpha\ \nabla_\alpha \qquad g_{\mu\nu}V(\ ). \tag{1.14}$$

As for the Klein-Gordon eq. (1.12), extremizing the Einstein Hilbert action with respect to will show that it remains the same after the system is coupled to gravity. Therefore, the set of equations governing the field coupled to gravity are eqs. (1.1) and eq. (1.12), which can be written as

$$\begin{aligned} R_{\mu\nu} \quad \frac{1}{2}g_{\mu\nu}R &= \kappa\left(\nabla_\mu\ \nabla_\nu \qquad \frac{1}{2}g_{\mu\nu}\nabla^\alpha\ \nabla_\alpha \qquad g_{\mu\nu}V(\ )\right), \\ \nabla_\mu\nabla^\mu\ &= \frac{dV}{d}. \end{aligned} \tag{1.15}$$

It should be noted that the above equations are insufficient to uniquely specify the system. This unfortunate ambiguity stems from the fact that there is no way to physically distinguish between two solutions of the system (1.15) related by a diffeomorphism. Indeed, there is no preferred coordinate system in general relativity, since the laws of physics should remain the same regardless of one's frame of reference. To state this somewhat more precisely, if reality is described by a manifold M and a set of tensor fields $T^{(i)}$ on M, then any two descriptions $(M, T^{(i)})$ and $(N, K^{(i)})$ related by a diffeomorphism $: M \to N$ have the same physical properties. Any physical statement one can make about the description $(M, T^{(i)})$ applies equally well to the description $(N, K^{(i)})$. Therefore, for all physical purposes, solutions related by diffeomorphism represent the same physical solution and are essentially indistinguishable. As such, if we wish to solve the system (1.15), we must select

one of the myriad of possible solutions to eqs. (1.15) by explicitly specifying a coordinate system (a gauge).[3]

1.3 Boson Stars

Put simply, boson stars are a class of mathematical objects in general relativity which result when a *complex* scalar field is coupled to gravity in the manner described in the previous section. Although they are relatively straightforward to define, their dynamics are highly nontrivial from a mathematical viewpoint, often exhibiting interesting behavior which deserves to be studied. However, it should be noted that boson stars are, as of writing, purely mathematical constructs – the question of their physical existence is currently unanswered and consequently motivates a portion of this project. But even if they do not exist in nature, they serve an important function as a simple model for compact objects. In this regard, they have very concrete advantages over the fluid neutron star model, as the governing equations cannot develop discontinuities and one does not need to worry about possible turbulence.

The origin of the boson star model traces back to the physicist John Wheeler in the 1950s. Originally, Wheeler intended to construct particle-like objects by coupling the electromagnetic field to gravity. In doing so, Wheeler managed to produce solutions to which he gave the name *geons*. Unfortunately, these solutions were markedly unstable, but they did form the basis for Kaup's formulation of the boson star, whereby a complex scalar field was substituted for the electromagnetic field. Kaup's idea has seen a number of augmentations since its proposal, and the result is a veritable boson star zoo. There are massive variety of different boson stars, ranging from charged boson stars, where the complex field is further coupled to the electromagnetic field, to Newtonian boson stars, where general relativity is eschewed in favor of Newtonian gravity. Some boson stars exhibit soliton-like behavior, where two stars moving in opposite directions may collide, interact in some nonlinear fashion, and then reform and recover their initial identities after collision. Indeed, the so-called

[3] See appendix A for further details.

\solitonic boson stars" and their properties are our primary interest in this project.

Coupling a complex scalar eld to gravity is done exactly as described in the previous section. We begin with a complex eld de ned over M,

$$= \ _R + i \ _C , \tag{1.16}$$

using the Einstein Hilbert action from the previous section,

$$S = \int_M \left[\frac{1}{2\kappa} R + L_M \right] \sqrt{-g}\, d^4x , \tag{1.17}$$

where the analogous matter Lagrangian L_M is given by

$$L_M \quad r^\mu \quad r_\mu \quad V(j \ j^2) . \tag{1.18}$$

From the action above, the Einstein eld equations become

$$\begin{aligned} R_{\mu\nu} \quad & \frac{1}{2} g_{\mu\nu} R = \kappa T_{\mu\nu} , \\ & T_{\mu\nu} \quad r_\mu \quad r_\nu \ + \ r_\mu \quad r_\nu \quad g_{\mu\nu}(r^\alpha \quad r_\alpha \ + V(j \ j^2)) . \end{aligned} \tag{1.19}$$

The Klein-Gordon equation for the complex scalar eld obtained from the action (1.17) is

$$r_\mu r^\mu \ = \frac{dV}{dj \ j^2} \quad . \tag{1.20}$$

Since the Klein-Gordon equation is complex, eq. (1.20) actually translates into two real equations for $_R$ and $_C$. In fact, since the eq. (1.20) exhibits $U(1)$ symmetry, i.e. symmetry under transformations $\ ! \ e^{i\theta}$, there exists a corresponding Noether current which is conversed by the dynamics of the system. This current is given by

$$J_\mu = i(\quad r_\mu \quad r_\mu \quad) , \tag{1.21}$$

which is divergenceless and hence satis es the conservation law

$$r_\mu J^\mu = 0 . \tag{1.22}$$

As a result, there is a corresponding conserved Noether charge associated with the system,

$$Q = \int g^{0\mu} J_\mu \sqrt{-g}\, d^3x , \tag{1.23}$$

where the integral is taken over a time slice of a foliation of the manifold M.

The speci c potential $V(j\ j^2)$ one assigns to a boson star plays a signi cant role in determining its properties. There are a number of common choices for the potential in the literature, ranging from the simple potentials associated with mini-boson stars to the more complicated potentials associated with solitonic boson stars. While our primary concern are the solitonic class of boson stars, our project will also examine two other important classes of boson stars,

1. **Mini-boson stars**: arguably the simplest boson star with a nontrivial potential. mini-boson stars arise when the potential is chosen to be

$$V(j\ j^2) \quad m^2 j\ j^2, \tag{1.24}$$

   where m is a constant describing the mass of the boson star. However, despite the simple potential, it is still possible for mini-boson stars to exhibit aforementioned soliton-like behavior, see [4].

2. **Massive boson stars**: similar to the mini-boson star potential, but the massive boson star model adds a higher order self-interaction term. This choice of potential was originally motivated by the additional self-interaction terms of the Heisenberg non-linear spinor equation, and was intended to model the interactions between desperate bosonic particles in a \geon" [22]. Explicitly, the potential is written as

$$V(j\ j^2) \quad m^2 j\ j^2 + \frac{1}{2}\lambda j\ j^4. \tag{1.25}$$

   A somewhat interesting fact about these types of stars is that they can still exhibit behavior signi cantly di erent from mini-boson stars even in the limit $\lambda\ !\ 0$. Moreover, for certain values of λ, it is possible to come close to the Chandrasekhar limit on the mass of the star [7].

In both of these models, the presence of gravity plays an important role, as it counteracts the dispersive nature of the Klein-Gordon equation and allows for the formation of con ned nondispersive solutions. If we were to remove gravity from the model, we would not expect

to be able to find confined nondispersive solutions for the above two classes of boson stars. Interestingly enough, this is one of the primary differences between the above models and the solitonic boson star model, where the potential is taken to be

$$V(|\Phi|^2) = m^2|\Phi|^2\left(1 - \frac{|\Phi|^2}{\sigma^2}\right) \tag{1.26}$$

Even in the non-gravitational regime, such objects can actually exhibit confined nondispersive solutions. Moreover, the model can exhibit a very specific class of static solutions referred to as thin-wall solutions, which can roughly be described as having a \shell-like" shape. We will explain these solutions in greater detail in the next section, but the reader should note that these solutions are ultimately critical to the objective of this project, as they exhibit the desired mass distribution we would require to produce the characteristic gravitational wave signal we desire. But before we examine these solitonic boson stars in greater detail, it is worth briefly digressing to the topic of Q-balls and Q-stars. Non-gravitational Q-ball models from particle physics can also form similar thin-wall solutions, which survive the transition into the gravitational regime from Q-balls to Q-stars. As we shall see in the following section, the ground states of solitonic boson stars are essentially Q-stars. The thin-wall solutions of interest have also been studied to some degree in the physics literature on Q-balls.

1.3.1 Q-balls, Q-stars, and Thin-Wall Solutions

A Q-ball is a defect structure of non-topological type from particle physics. In general, defect structures may be either topological or non-topological in nature. The distinction comes from the fact that topological defects carry a certain topological current, which is conserved due the topological properties of the solutions. For instance, one may consider the example of a field theory in $\mathbb{R}^n$ with a nontrivial vacuum manifold $\mathcal{V}$[4] (as an example, we may have $\mathcal{V} = U(1)$). For a given field Φ in this theory, one may view the values that Φ takes on at infinity as a map $j_\Phi : S^{n-1} \to \mathcal{V}$ and hence a member of the homotopy group $\pi_{n-1}(\mathcal{V})$. The map j_Φ gives us a notion of a topological current which can be associated

[4] The manifold $\mathcal{V}$ may be thought of as the set of points at which the potential of the field theory is zero.

to . In theory, because distinct members of the homotopy group cannot be continuously deformed into one another, this means that we should expect topological defects, i.e. elds which correspond to nontrivial members of the homotopy group $\pi_{n\ 1}(V)$, to be topologically stable against perturbations.

In contrast, some defect structures are non-topological, which means they do not have such topological currents to stabilize them. However, there are cases in which these defect structures can still be stabilized. Q-balls fall into this latter class. Succinctly, Q-balls are ground state con gurations in scalar eld theories with a conserved $U(1)$-charge. They have enjoyed some recognition as candidates for collisional dark matter, owing to the fact that they satisfy requisite cross-section conditions for larger range of masses than pointlike particles and, in certain situations, they can scatter inelastically [16].

For the moment, let us take a step back and consider a complex scalar eld in at space. Let the Lagrangian density of the eld be the non-gravitational analogue of what we examined in the previous section,

$$L(\ ,\partial\ )\quad \frac{1}{2}\partial_\mu\quad \partial^\mu\qquad V(j\ j^2)\,, \tag{1.27}$$

where the potential $V(j\ j^2)$ is required to have a global minimum at 0 and be invariant under $U(1)$ transformations. There is a corresponding Noether charge resulting from $U(1)$-symmetry,

$$Q = \frac{1}{2i}\int\qquad -\qquad -\ d^3x\,, \tag{1.28}$$

and a corresponding energy from time invariance symmetry,

$$E = \int \left[j\text{-}j^2 + j\,r\quad j^2 + V(j\ j^2)\right]\,dx^3\,. \tag{1.29}$$

The Q-ball solution to the system de ned by (1.27) is de ned as the minimum energy con guration in the sector of xed charge. It turns out that nding the minimum energy con guration for a given charge sector is surprisingly straightforward and can be shown to be of the oscillating spherically symmetric form [6, 18], i.e. given by

$$(x,t) = \varphi(r)e^{i\omega t}\,, \tag{1.30}$$

where ω is the frequency of oscillation and φ is real and time independent. Under this ansatz, the quantities (1.28) and (1.29) become

$$\begin{aligned} Q &= 4\pi\omega \int_0^1 r^2\varphi^2\, dr\,, \\ E &= 4\pi \int_0^1 \left[\omega^2\varphi^2 + |r\varphi|^2 + V(\varphi^2)\right] dr\,. \end{aligned} \tag{1.31}$$

For a fixed frequency ω, the ansatz (1.30) and Lagrangian (1.27) give an ordinary differential equation for the radial amplitude φ,

$$\frac{d^2\varphi}{dr^2} + \frac{2}{r}\frac{d\varphi}{dr} = \varphi\frac{dV(\varphi^2)}{d(\varphi^2)} - \omega^2\varphi\,. \tag{1.32}$$

Q-balls for a specific frequency are obtained by solving the above equation with the boundary conditions $\varphi'(0) = 0$ and $\varphi(1) = 0$.

Of course, the shape, energy, charge, and stability of a Q-ball are strongly influenced by the choice of potential V. Indeed, the dispersive nature of the governing equation which results from Lagrangian (1.27) suggests that it would be difficult to even find Q-balls for very simple potentials. As such, the choice of potential V is very important, and can give rise to different salient features – in particular, the aforementioned thin-wall behavior.

There are a number of common Q-ball types which crop up in the literature as a result of the choice of V. Typically, the shape of Q-balls falls into one of two types. The Q-ball may posses a well-defined edge, that is, a boundary localized in a thin narrow region. In this case, the Q-ball is referred to as a thin-wall Q-ball (or a Type I Q-ball). If the Q-ball doesn't have this feature, it is referred to as thick-wall, which can be further classified into a Type II or a Type III respectively, depending on whether the potential V is asymptotically flat or logarithmic. Naturally, the Type I Q-balls are the type most relevant to this project, since they have the approximate distribution of mass we would like for our black hole mimic candidate. Such thin-wall Q-balls arise for any suitable potential $V(\ )$, for which Q-balls do exist, and which grows faster than ^{2} in the $\ \to 1$ limit [9]. The thin-wall Q-ball solutions of this type then approximately take the profile

$$\varphi(r) \quad \varphi_0 H(r \quad R)\,, \tag{1.33}$$

where H is the Heaviside step function. The Q-ball solutions for potentials of this type in fact tend toward this Heaviside limit as the frequency ω becomes small enough, and near this limit there is a linear relationship between the energy and charge of Q-balls [23]. Correspondingly, if the potential V grows slower than ^{2}, we obtain thick-wall Q-balls.

When a Q-ball of the form above is coupled to gravity, the result is referred to as a Q-star. Remarkably, some of the interesting aforementioned features of Type I Q-balls carry over into the gravitational regime. In the literature on Q-stars, e.g. [28], the potential function is usually taken to be

$$V(j\ \ j^2)\quad \frac{m^2}{2}j\ \ j^2\quad \frac{\alpha m^{4\ \ p}}{p}j\ \ j^p + \frac{\lambda m^{4\ \ q}}{q}j\ \ j^q . \tag{1.34}$$

The two popular choices for the integer parameters p and q are $p = 3, q = 4$ (the 2-3-4 potential) and $p = 4, q = 6$ (the 2-4-6 potential). The motivation for these choices lies in the fact that these potentials still produce Q-balls in the at space limit, whereas other choices of potential may produce systems where the presence of gravity is necessary to counterbalance the dispersive nature of the governing equations (e.g. $V = m^2 j\ \ j^2$), which means the at space limit does not exist. With correct choice of parameters, it is easy to see that the latter 2-4-6 potential is essentially equivalent to the solitonic boson star potential (1.26). For Q-stars, we carry over spherical symmetry from the non-gravitation regime, and let the eld and the metric ds^2 take on the forms

$$\begin{aligned} (r,t) &= \varphi(r)e^{i\omega t}, \\ ds^2 &= \quad \alpha(r)^2\,dt^2 + a(r)^2\,dr^2 + r^2\,d\ \ ^2 . \end{aligned} \tag{1.35}$$

The relativistic analogues of the charge and energy quantities (1.28) and (1.29) then become

$$\begin{aligned} Q &= 4\pi\omega \int_0^1 r^2 \frac{a}{\alpha}\varphi\, dr, \\ M &= 4\pi \int_0^1 r^2 \left[\frac{\omega^2\varphi^2}{2\alpha^2} + \frac{\varphi^{\prime 2}}{2a^2} + V(\varphi^2)\right] dr, \end{aligned} \tag{1.36}$$

see [28]. Just as in the at space case, there are similar conditions required for the formation of Q-stars. In particular, one may consider the ω-dependent potential V_ω, de ned as

$$V_\omega(a^2,\varphi)\quad \frac{1}{2}V(\varphi^2)\quad \frac{1}{2}\frac{\omega^2}{a^2}\varphi^2 , \tag{1.37}$$

where a is the radial component of the metric in (1.35). For Q-stars to exist, it is necessary for there to exist a non-zero minimum φ_+ of the ω-dependent potential V_ω that satisfies the condition

$$V_\omega(a^2, \varphi_+) < V_\omega(a^2, 0)\,, \tag{1.38}$$

see [23]. This condition places constraints on both the value of the frequency ω and also the radial component a of the metric.

In the gravitational regime, it is also possible to find thin-wall Q-stars. These occur when the height of the barrier between the minima of V_ω at 0 and φ_+ is significantly larger than the difference between the minima [23]. If this condition is met, the field forms a bubble of some radius R. In the interior of the bubble, the field is approximately constant, and on the exterior of the bubble, the field is virtually zero. In between, on the \surface" of the bubble, there is a thin region where the field undergoes a sharp transition. Thus, the field again has the approximate profile of eq. (1.33). One should note, however, that while the field is approximately constant on the inside of the bubble, the components α and a of the metric are not. Instead, they are monotonic.

One can solve for Q-stars by plugging the ansatz (1.30) into the Einstein field equations and the Klein-Gordon equation. The result will be a system of ordinary differential equations in the variable r for the fields φ, α, and a. Like in the flat space limit, we also prescribe the boundary conditions $\varphi'(0) = 0$ and $\varphi(r \to \infty) = 0$. This is precisely how one may solve for the ground states of boson stars, and we will cover the numerical aspects of such a computation later in this paper.

We are particularly interested in the dynamical and structural properties of such thin-wall solutions for solitonic boson stars, chiefly whether they are stable with respect to small perturbations of the field. A study of these properties would be important in determining whether the thin-wall ground states of solitonic boson stars are viable candidates for our black hole mimic.

1.3.2 Boson Stars Driven to the Brink of Black Hole Formation

It has been observed through a number of numerical studies over the course of the 1990s that models of gravitational collapse exhibit interesting \critical solutions" at the threshold of black hole formation. These types of critical solutions are prevalent in the theory of gravitational collapse, and are present even in very simple models, such as a real scalar eld coupled to gravity in spherical symmetry [5]. As expected, critical solutions occur in any one-parameter family of initial data which interpolates between black hole formation from the initial data at one extreme and dispersion of the matter to in nity at large times at the other extreme. Indeed, when the parameter governing the one-parameter family is given by p, there is invariably a critical value $p = p$ which delineates the threshold of black hole formation. Perhaps the most striking thing about these solutions is that the critical solution at p is essentially independent of the choice of one-parameter family [14]. The corresponding threshold for black hole formation exhibits a surprising amount of simplicity in its structure { but an in-depth discussion on this topic is beyond the scope of this paper. Regardless, the features exhibited by these solutions are referred to as \critical phenomena" and have been quite well studied. If the reader is so inclined, he/she may see [13] for a more detailed overview of the subject.

In their 2000 paper, Hawley and Choptuik [14] studied the critical phenomena which occurs at the threshold of black hole formation for the ground states of mini-boson stars. They use a gravitational model consisting of a complex scalar eld $_C$ (the boson star) and a massless real scalar eld $_R$ (a small perturbation) and vary the parameter of a family of one-parameter initial data con gurations to locate the threshold of black hole formation, e ectively performing a binary search in the parameter space to hone in on the critical solution. The boson star begins in a static ground state and the initial real scalar eld $_R$ is taken to be either a Gaussian or a Kink at some large radius r_0 signi cantly greater than the radius of the boson star. The initial data for the real scalar eld $_R$ is taken so that the eld excitation moves inwards, eventually perturbing the boson star and triggering critical behavior. Note that the initial amplitude of the eld $_R$ is critically

important here, since it determines the magnitude of the perturbation to the boson star $_C$. Indeed, the amplitude of the perturbation pulse $_R$ is the parameter Hawley and Choptuik tune to arrive at their critical solutions. It should be mentioned that while these critical solutions are clearly unstable { as even slight deviations from the correct parameters can cause drastically di erent outcomes { the solutions are unstable in a very minimal sense. It can be shown using linear perturbation theory that the instability is the result of a singe unstable mode [10, 15]. Hence, performing the above search of the parameter space essentially amounts to carefully tuning the initial data such that the amplitude for this unstable mode tends to zero.

Now let us turn to the mathematical details of Hawley and Choptuik's scalar eld model. As we mentioned, their model includes a complex scalar eld $_C = _1 + i\ _2$ for their mini-boson star as well as a massless real scalar eld $_R = _3$. In the model, the elds have no direct interaction between each other, the only indirect interaction between the two elds comes through the gravitational eld. Following this description, the action for the system is given by

$$S = \int_M \left[\frac{1}{2\kappa}R + L_C(\ _C, r\ _C) + L_R(\ _R, r\ _R)\right] p\overline{-g}\, d^4x\,, \tag{1.39}$$

where the individual Lagrangian densities L_C and L_R for the elds $_C$ and $_R$ are given by

$$\begin{aligned} L_C(\ _C, r\ _C) &\quad r^\mu\ _C\, r_\mu\ _C\quad m^2 j\ _C j^2\,,\\ L_R(\ _R, r\ _R) &\quad r^\mu\ _R\, r_\mu\ _R\,. \end{aligned} \tag{1.40}$$

The resulting Einstein equations are

$$R_{\mu\nu}\quad \frac{1}{2}g_{\mu\nu}R = \kappa(T^C_{\mu\nu}(\ _C) + T^R_{\mu\nu}(\ _R))\,, \tag{1.41}$$

where the stress-energy tensors $T^C_{\mu\nu}$ and $T^R_{\mu\nu}$ are given by

$$\begin{aligned} T^C_{\mu\nu}(\ _C) &= r_\mu\ _C\, r_\nu\ _C + r_\mu\ _C\, r_\nu\ _C\quad g_{\mu\nu}(r_\rho\ _C\, r^\rho\ _C + m^2 j\ _C j^2)\,,\\ T^R_{\mu\nu}(\ _R) &= 2\, r_\mu\ _R\, r_\nu\ _R\quad g_{\mu\nu}\, r_\rho\ _R\, r^\rho\ _R\,. \end{aligned} \tag{1.42}$$

And nally, the Klein-Gordon equations governing the motion of the elds are given by

$$\begin{aligned} r_\mu r^\mu \ _C &= m^2 \ _C , \\ r_\mu r^\mu \ _R &= 0 . \end{aligned} \tag{1.43}$$

Now, consider the system in spherical symmetry, where we use Schwarzschild-like \polar-areal" coordinates,

$$ds^2 = \ \alpha^2(t,r)\,dt^2 + a^2(t,r)\,dr^2 + r^2\,d \ \ . \tag{1.44}$$

The reader may note that all of the above equations place both space and time on equal footing, making it unclear how exactly one goes about evolving initial data on the manifold M. To deal with this problem, we make use of the \3 + 1" ADM formalism (see appendix A or reference [8]). Assuming that the spacetime M can be foliated into space-like time slices $_t$ parametrized by a time coordinate t and using the implicit choice of gauge in eq. (1.44), we can decompose the above equations into a complete set of hyperbolic evolution equations and elliptic constraint equations.

First o , to end up with a system of rst order di erential equations, we de ne the following variables:

$$\begin{aligned} \xi_1 \quad & \overset{0}{1}, \quad & 1 \quad & \frac{a}{\alpha} - 1 , \\ \xi_2 \quad & \overset{0}{2}, \quad & 2 \quad & \frac{a}{\alpha} - 2 , \\ \xi_3 \quad & \overset{0}{3}, \quad & 3 \quad & \frac{a}{\alpha} - 3 , \end{aligned} \tag{1.45}$$

where ^{0} denotes partial di erentiation in r and denotes partial di erentiation in t. Now, rewrite the Einstein eqs. (1.39) in the form $A_{\mu\nu} = 0$. The Hamiltonian constraint can be computed from expanding the identity $ra^2A_{tt}/(2\alpha^2) = 0$, resulting in

$$\frac{a^0}{a} = \frac{1 \quad a^2}{2r} + \kappa\frac{r}{2}\left[\ \overset{2}{1} + \ \ \overset{2}{2} + \ \ \overset{2}{3} + \xi_1^2 + \xi_2^2 + \xi_3^2 + a(\ \overset{2}{1} + \ \ \overset{2}{2})\right] . \tag{1.46}$$

On the other hand, the so-called slicing condition can be computed from expanding the identity $rA_{rr}/2 \quad ra^2A_{tt}/(2\alpha^2) = 0$,

$$\frac{\alpha^0}{\alpha} = \frac{a^2 \quad 1}{r} + \frac{a^0}{a} \quad \kappa a^2 r(\ \overset{2}{1} + \ \ \overset{2}{2}) . \tag{1.47}$$

And nally, the Klein Gordon eqs. (1.43) can be expanded into

$$\dot{\Psi}_k = 3\frac{\partial}{\partial r^3}\left(\frac{r^2\alpha}{a}\xi_k\right)' \quad \alpha a \quad {}_k(1 \quad \delta_{3k}) . \tag{1.48}$$

Additional equations for the radial derivative of the scalar elds ${}_k$ as well as the scalar elds themselves are now taken from the de nitions (1.45) of ξ_k,

$$\begin{aligned} \xi_k &= \left(\frac{\alpha}{a} \quad {}_k\right)' , \\ {}_k &= \int_0^r \xi_k \, dr . \end{aligned} \tag{1.49}$$

We will give a full overview of the numerical methods used to solve equations like these in chapter 3.

As previously mentioned, our initial data for the eld ${}_R$ is simply an ingoing pulse at a large radius, either a Gaussian or a Kink with some small amplitude. On the other hand, the initial data for the eld ${}_C$ can be computed via a method similar to the one used compute Q-balls in at space from section 1.3.1. First, as in the Q-ball case, we consider the boson star *ansatz* given by the now familiar rotating phase expression

$${}_C(t, r) = \varphi(r)e^{i\omega t} , \tag{1.50}$$

where φ is the real-valued pro le of the star, and ω is the real-valued frequency of oscillation. Inserting the ansatz (1.50) into the above di erential eqs. (1.46) through (1.48) gives a system of three ordinary di erential equations for the elds $f\varphi, \alpha, ag$ in terms of the variable r, analogous to the eq. (1.32) for Q-balls. Similarly, to ensure spherical symmetry and vanishing of the eld at in nity, one prescribes the boundary conditions given by

$$\begin{aligned} \varphi'(0) = 0 , \qquad a'(0) = 0 , \\ \varphi(r \; ! \; 1) = 0 , \qquad \alpha'(0) = 0 . \end{aligned} \tag{1.51}$$

In practice, to ensure $\varphi(1) = 0$, one uses a \shooting" method. That is, instead of specifying φ at the far end of the computation region, one instead uses $\varphi(0)$ as a parameter and adjusts the parameter via binary search until the condition $\varphi(1) = 0$ is met. Alternatively, one can x the parameter $\varphi(0)$ and instead perform a binary search in the frequency ω

until the condition $\varphi(1) = 0$ is met. The latter is our preferred method. We will discuss the aspects of computing initial data further in chapter 2. Once initial data for the fields $_C$ and $_R$ has been specified, the elliptic constraint eqs. (1.46) and (1.47) fix the initial geometry $a(0, r)$ and $\alpha(0, r)$.

When considering the results of simulations, it is often useful to associate a mass aspect function to both the complex field $_C$ and the real field $_R$. Unfortunately, there is not a good notion of "mass" for the individual fields $_C$ and $_R$ while the two are subject to nonlinear interactions between each other. Nonetheless, to be able to talk unambiguously about the "mass" exchanged between the incoming perturbation $_R$ and the boson star, it is useful to define some weak notion of these concepts. In particular, Birchoff's theorem tells us that, in any vacuum region, the mass enclosed by a sphere of radius r at time t is given by the mass aspect function

$$M(t, r) = \frac{r}{2}\left(1 \quad \frac{1}{a^2}\right) . \tag{1.52}$$

In our choice of coordinates, the derivative of the mass aspect function (i.e. the "mass density" at a particular radius), can be written in terms of the local energy density $\rho(t, r)$ by

$$\frac{\partial M}{\partial r} = r^2 \rho(t, r) , \tag{1.53}$$

where ρ takes the form

$$\rho(t, r) = \frac{1}{2a^2}\left[\ {}^2_1 + \ {}^2_2 + \xi_1^2 + \xi_2^2 + a^2\left(\ {}^2_1 + \ {}^2_2\right)\right] + \frac{1}{2a^2}\left[\ {}^2_3 + \xi_3^2\right] . \tag{1.54}$$

Notice that the expression for local energy density has been separated into two terms. On the left are the terms belonging to the complex scalar field $_C$, and on the right are the terms belonging to the real scalar field $_R$. In the case where the supports of the fields $_C$ and $_R$ do not overlap one another, one can separate the above local energy density into a local energy density for $_C$,

$$\rho_C(t, r) \quad \frac{1}{2a^2}\left[\ {}^2_1 + \ {}^2_2 + \xi_1^2 + \xi_2^2 + a^2\left(\ {}^2_1 + \ {}^2_2\right)\right] , \tag{1.55}$$

and a local energy density for the eld $_R$,

$$\rho_R(t,r) \quad \frac{1}{2a^2}\left[\ \ ^2_3 + \xi_3^2\right] . \tag{1.56}$$

We can de ne respective mass aspect functions for the individual elds by integrating the above densities,

$$M_C(t,r) \quad \int_0^r r^2\rho_C\, dr \qquad M_R(t,r) \quad \int_0^r r^2\rho_R\, dr \tag{1.57}$$

One should note that in non-vacuum regions, the above mass aspect functions may not necessarily have any direct physical meaning. Thus, M, M_C, and M_R should only be associated with a physical mass when the radius r is large enough such that the entire system is contained inside. However, note that $M = M_C + M_R$ is conserved at large radii, therefore examining M_C and M_R over the evolution of the system should allow us to get an idea of the exchange of energy between the two elds.

It is known from [12, 17] that mini-boson stars exhibit a critical value c of the central eld modulus $\varphi(0)$ marking the transition between mini-boson stars which are stable with respect to extremely small perturbations and those which are not. Moreover, the simulations in [27] indicate that the latter branch of solutions either eventually collapse to a black hole when perturbed, or they radiate away energy and collapse to solutions on the stable branch. In the simulations of Hawley and Choptuik above, more or less the same thing happens, the incoming perturbation given by $_R$ has the e ect of shifting the boson star from this stable branch of solutions onto the unstable branch, at which point the star either collapses to a black hole or eventually collapses back to a solution on the stable branch. And as one gets closer to the critical solution at which the black hole forms, the time it takes for the unstable boson star to collapse increases. An example of a simulation by Hawley and Choptuik is seen in gures 1.2, 1.3, and 1.4, where we see the boson star shift onto the unstable branch for a period of time until it nally collapses.

Our ultimate goal in this project is to perform a similar analysis to Hawley and Choptuik [14] above, except for the thin-wall ground states of solitonic boson stars that we touched upon in section 1.3.1. The underlying rational is quite natural: if one wants to ask whether

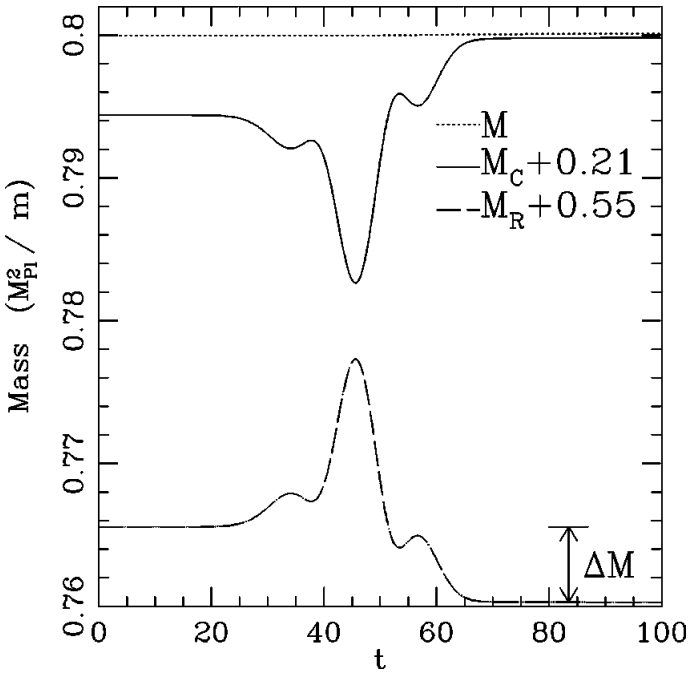

Figure 1.2: Results of a simulation from [14] near critical solution, shows the evolution of M_C and M_R at large radii over time. The solid line is the mass of the boson star $_C$, and the dashed line is the mass of the perturbation $_R$. As we can see, there is a period from t 20 to t 60 where the two elds interact before the perturbation $_R$ radiates back o to in nity, resulting in a nal exchange of energy M between the real scalar eld and the boson star.

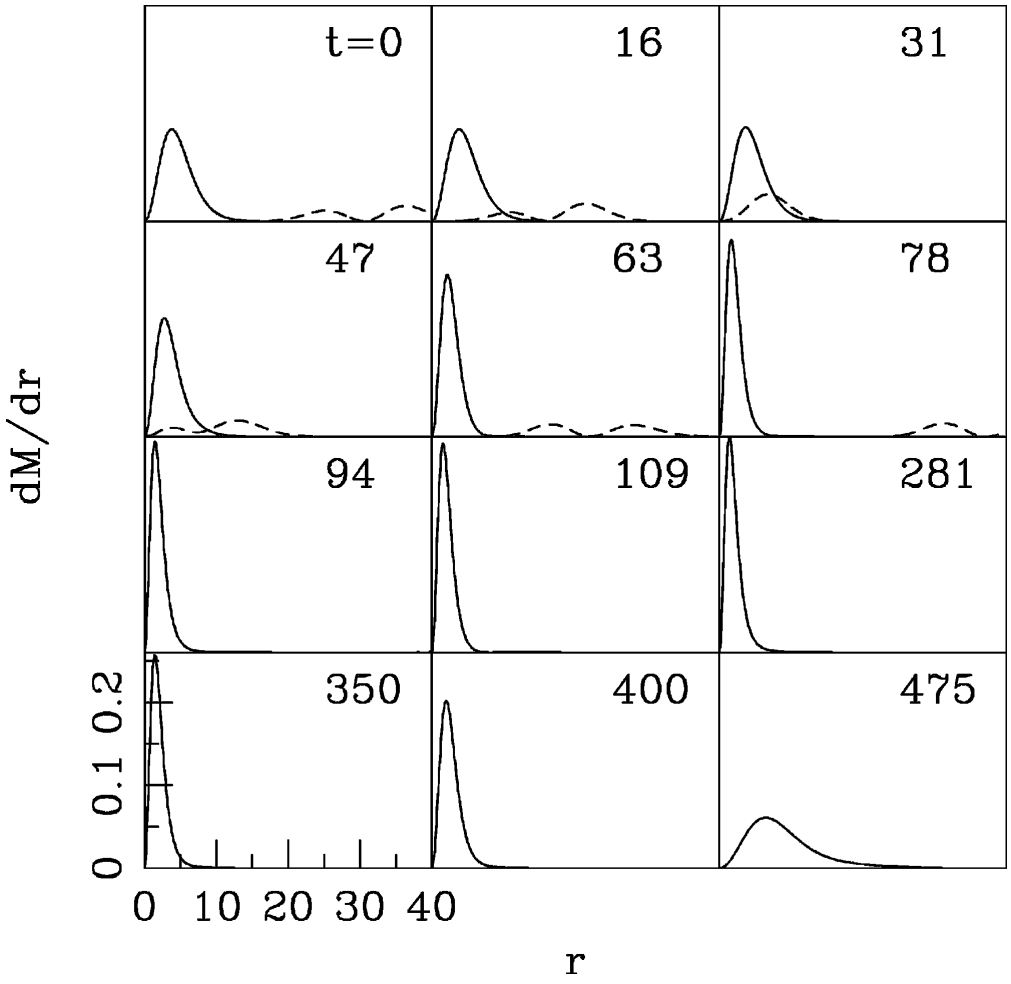

Figure 1.3: Results of a simulation from [14] near critical solution. The solid graph denotes the mass density $\partial M_C/\partial r$ of the complex scalar field $_C$, and dashed graph denotes mass density $\partial M_R/\partial r$ of the real scalar field $_R$. The boson star initially has central modulus value $\varphi(0) = 0.04\sqrt{4\pi}$ and mass $M_C = 0.59 M_{Pl}^2/m$. Note that the real scalar field enters the bulk of the boson star at t 15 and leaves the boson star at about t 50. After perturbation, boson stars collapse into a more compact form as seen above, oscillating until they either form a black hole or disperse. In this case, the latter happens at about t 475.

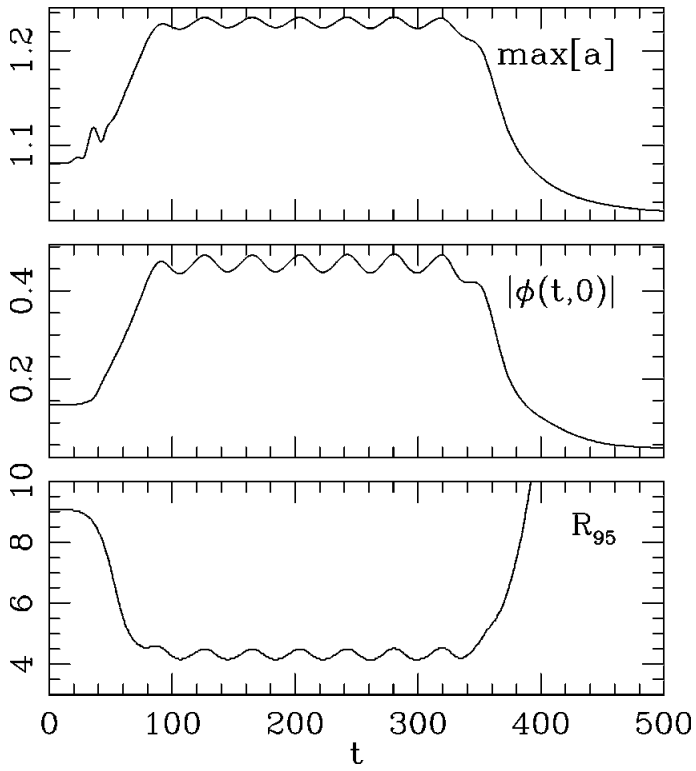

Figure 1.4: Results of a simulation from [14] near the critical solution. Shown above are the maximum value of the function a, the central modulus of the complex scalar field $|\phi_C(t,0)|$, and the radius of the boson star as they evolve over time. Note that the boson star is shifted from the stable branch to the unstable branch when it starts interacting with the incoming perturbation ϕ_R. As it remains on the unstable branch, the star oscillates for a period of time until it collapses back onto another point on the stable branch.

these thin-wall solutions can be used to mimic measured gravitational wave signals, it is critical to examine their stability properties.

Chapter 2

Boson Star Ground States

A signi cant portion of this project was devoted to developing a numerical code to nd the ground states of mini, massive, and solitonic boson stars. In this chapter, we will detail both the algorithms used to compute these states as well as report a number of results and observations from the output of the numerical code. These observations coincide with computations done in [20]. The overall goal here is to be provide initial data for numerical perturbation in chapter 3 and also to obtain a better understanding of the practical considerations involved in nding these states. Of particular interest are the thin-wall ground states introduced in section 1.3.1 of the previous chapter. Using high-precision- oating point computation, we are able to isolate these ground states and give a few remarks about their behavior. We observe that these thin-wall states begin to arise when the central eld value of the boson star becomes larger than the degenerate vacuum magnitude σ of the corresponding solitonic potential. Moreover, there seems to be a small range above this value where the thin-wall ground state of the star is hidden by a more conventional Gaussian-like ground state, in the sense that any change to the frequency ω of the star used to solve the underlying ordinary di erential equations will cause the solution to diverge in one direction only, making it di cult to nd these states via binary search in the frequency ω without special-purpose code. As desired, the thin-wall ground states we nd are quite compact,

with a radius-mass ratio of R/M 3.5.[1]

2.1 Algorithm for Numerical Computation

The algorithm described in this section is based on the preliminaries of section 1.3.2. To nd stationary states of boson stars with some arbitrary potential $V(j \ _C j^2)$, we look for solutions to the eld equations in spherical symmetry under the rotating phase ansatz

$$(r,t) = \varphi(r)e^{i\omega t}. \tag{2.1}$$

Taking the same spherically symmetric metric as in section 1.3.2 with no shift vector,

$$ds^2 = \alpha^2(r,t)\,dt^2 + a^2(r,t)\,dr^2 + r^2\,d\ ^2. \tag{2.2}$$

The Einstein equations and Klein-Gordon equations governing the system read

$$\begin{aligned} R_{\mu\nu} \quad \frac{1}{2}g_{\mu\nu}R &= \kappa\left[r_\mu \ _C \, r_\nu \ _C + r_\mu \ _C \, r_\nu \ _C \quad g_{\mu\nu}(r_\rho \ _C \, r^\rho \ _C + V(j \ _C j^2))\right], \\ r_\mu r^\mu \ _C &= \frac{dV}{dj \ _C j^2} \ _C . \end{aligned} \tag{2.3}$$

We now introduce the auxiliary variables

$$\begin{aligned} \xi_1 \quad {}^{0}_{1}, \qquad & \xi_2 \quad {}^{0}_{2}, \\ {}_1 \quad \frac{a}{\alpha} - 1, \qquad & {}_2 \quad \frac{a}{\alpha} - 2. \end{aligned} \tag{2.4}$$

Expanding the eqs. (2.3) for a single complex scalar eld $_C$ in the same manner as in section 1.3.2 will give the following equations:

$$\begin{aligned} \frac{a^0}{a} &= \frac{1 \quad a^2}{2r} + \kappa\frac{r}{2}\left[\ {}^{2}_{1} + \ {}^{2}_{2} + \xi_1^2 + \xi_2^2 + aV(j \ _C j^2)\right], \\ \frac{\alpha^0}{\alpha} &= \frac{a^2 \quad 1}{r} + \frac{a^0}{a} \quad \kappa a^2 r V(j \ _C j^2), \\ - _k &= 3\frac{\partial}{\partial r^3}\left(\frac{r^2\alpha}{a}\xi_k\right)^0 \quad \alpha a\frac{dV}{dj \ _C j^2} \ _k . \end{aligned} \tag{2.5}$$

Our goal is to nd a numerical solution to the above system (2.5) using the ansatz (2.1).

[1] for reference, a Schwarzschild black hole has $R/M = 2$

2.1.1 Numerically Integrating the Differential Equations Outwards

Performing the substitutions $_1 \; ! \; \varphi\cos(\omega t)$ and $_2 \; ! \; \varphi\sin(\omega t)$ and dropping the time dependence of α and a, we recover a collection of three coupled ordinary di erential equations in the variable r for the eld variables $f\varphi, a, \alpha g$,

$$\begin{aligned}
\frac{a^{\prime}}{a} &= \frac{1 \quad a^2}{2r} + \frac{\kappa r}{2}\left[\frac{\omega^2 a^2}{\alpha^2}\varphi^2 + (\varphi^{\prime})^2 + a^2 V\left(\varphi^2\right)\right], \\
\frac{\alpha^{\prime}}{\alpha} &= \frac{a^2 \quad 1}{r} + \frac{a^{\prime}}{a} \quad \kappa a^2 r V(\varphi^2), \\
\frac{\omega^2 a\varphi}{\alpha} &= \frac{r\alpha a^{\prime}\varphi^{\prime} \quad r\alpha^{\prime} a\varphi \quad r\alpha a\varphi^{\prime\prime} \quad 2\alpha a\varphi^{\prime}}{ra^2} + a\alpha\frac{dV}{d\varphi^2}\varphi .
\end{aligned} \tag{2.6}$$

We solve these equations using a fourth order Runge-Kutta scheme. First, we convert the system of three equations above into four rst-order equations by adding the auxiliary variable ξ where $\xi = \varphi^{\prime}$ and performing the appropriate substitutions in the third equation above to remove all spatial derivatives of φ. Once this has been done, it is simple to solve for the spatial derivatives of each of the variables independently, yielding the set of four equations,

$$\begin{aligned}
\frac{da}{dr} &= \frac{a \quad a^3}{2r} + \frac{\kappa r}{2}\left[\frac{\omega^2 a^3\varphi^2}{\alpha^2} + a\xi^2 + a^3 V(\varphi^2)\right], \\
\frac{d\alpha}{dr} &= \frac{a^2\alpha^2 \quad \alpha}{2r} + \frac{\kappa r}{2}\left[\frac{\omega^2 a^2\varphi^2}{\alpha} + \alpha\xi^2 \quad a^2\alpha V(\varphi^2)\right], \\
\frac{d\varphi}{dr} &= \xi , \\
\frac{d\xi}{dr} &= \quad \frac{\xi + \alpha^2\xi}{r} \quad \frac{\omega^2 a^2\varphi}{\alpha^2} + r\kappa a^2\xi V(\varphi^2) + a^2\frac{dV}{d\varphi^2}\varphi .
\end{aligned} \tag{2.7}$$

Integrating this system out from a set of initial data at some $r = R$ can then be done via RK4. Let $\vec{y} \quad (a, \alpha, \varphi, \xi)$ be the vector of variables, then the above equations can be written in the vector form

$$\frac{d\vec{y}}{dr} = F(r, \vec{y}) . \tag{2.8}$$

To compute a numerical solution to this di erential equation, we discretize the region of integration with some grid spacing h. Let $\vec{y}_i$ denote our discrete approximations to the true

solution $\vec{y}$ at the grid point i. We start by assigning our initial data,

$$\begin{aligned} \vec{y}_0 &\quad \vec{y}(R)\,, \\ r_0 &\quad R\,, \end{aligned} \tag{2.9}$$

where the symbol is used to denote assignment. We then successively compute $\vec{y}_i$ using the following RK4 scheme,

$$\begin{aligned} \vec{y}_{i+1} &\quad \vec{y}_i + \frac{h}{6}(\vec{k}_1 + 2\vec{k}_2 + 2\vec{k}_3 + \vec{k}_4)\,, \\ r_{i+1} &\quad r_i + h\,, \end{aligned} \tag{2.10}$$

where the vectors $\vec{k}_1, \vec{k}_2, \vec{k}_3, \vec{k}_4$ are given by

$$\begin{aligned} \vec{k}_1 &\quad F(r_i, \vec{y}_n)\,, \\ \vec{k}_2 &\quad F\left(r_i + \frac{h}{2}, \vec{y}_i + \frac{h}{2}\vec{k}_1\right)\,, \\ \vec{k}_3 &\quad F\left(r_i + \frac{h}{2}, \vec{y}_i + \frac{h}{2}\vec{k}_2\right)\,, \\ \vec{k}_4 &\quad F\left(r_i + h, \vec{y}_i + h\vec{k}_3\right)\,. \end{aligned} \tag{2.11}$$

2.1.2 Integration From the Origin

Due to the presence of r in the denominator of some of the terms in the eqs. (2.7), integrating the system starting from the origin $R = 0$ requires some special care to avoid the problem of dividing by zero. This is done by taking the limit of the eqs. (2.7) as $r \to 0$, and using the initial values of the fields variables to replace quotients with r by derivatives in the fields variables. For our initial values, we take

$$a(0) = 1\,, \qquad \alpha(0) = 1\,, \qquad \xi(0) = 0\,, \tag{2.12}$$

where $\xi(0)$ must be zero for φ to be a differentiable function in spherical symmetry at the origin, and a and α are chosen this way for normalization purposes. Spherical symmetry and differentiability also tell us that we must have $a'(0) = 0$ and $\alpha'(0) = 0$, and indeed one can derive this from the system (2.7) and the initial values (2.12). Furthermore, since we

know $\varphi^{\prime}(0) = 0$, it simply remains to compute the value of $\xi^{\prime}(0)$. Using these initial values to take the $r \to 0$ limit of the last equation in (2.7) now gives

$$\xi^{\prime} = -(1 + \alpha^2)\xi^{\prime} - \frac{\omega^2 a^2 \varphi}{\alpha^2} + a^2 \frac{dV}{d\varphi^2}\varphi \,. \tag{2.13}$$

Using the initial values from (2.12) and solving for $\xi^{\prime}$ yields

$$\begin{aligned} \frac{da}{dr} &= 0 \,, \\ \frac{d\alpha}{dr} &= 0 \,, \\ \frac{d\varphi}{dr} &= 0 \,, \\ \frac{d\xi}{dr} &= \frac{\varphi}{3}\left(-\omega^2 + \frac{dV}{d\varphi^2}\right) \,. \end{aligned} \tag{2.14}$$

Eliminating the arithmetic problems at $r = 0$ is now simply a matter of using the formulation (2.14) of $F(r, \vec{y})$ near the origin and the original formulation (2.7) of $F(r, \vec{y})$ elsewhere.

2.1.3 Finding Ground States

Now that we have shown in the above sections how to compute numerical solutions to the ordinary differential equations for a static boson star, it is time to turn to the problem of finding the ground states of boson stars. In general, for an arbitrary frequency ω, the solution to system (2.7) grows exponentially in the $r \to \infty$ limit, due to the presence of an exponentially growing mode which dominates in the large radius limit. However, for a "physical" solution to these equations,[2] we demand that the solution be localized in space and satisfy

$$\varphi(r \to \infty) = 0 \,. \tag{2.15}$$

Accordingly, the metric should also be Minkowski at large radii. For each initial value of φ at $r = 0$, the above condition (2.15) is satisfied by a discrete spectrum of eigenfrequencies ω [20]. At these frequencies, the aforementioned exponentially growing mode, which normally

[2] "physical" is meant in a very weak sense here. As "physical" as one can be with a purely hypothetical mathematical object.

dominates the solution, is tuned away. The result is a solution whose pro le is localized in space. The ground state of the boson star is designated as the solution with the lowest eigenfrequency, or equivalently, the solution whose pro le $\varphi(r)$ has no zeroes. The overtone solutions corresponding to the higher eigenfrequencies are the excited states of the boson star. In practice, these excited states decay to ground states through the emission of scalar and gravitational radiation [11].

The thin-wall stars we are interested in manifest as ground states of solitonic boson stars in a speci c regime of the initial eld value parameter $\varphi(0)$. Hence, computing ground states for boson stars is not only important for providing initial data for dynamical simulations, but also for understanding the properties and structure of these thin-wall stars. Given a speci ed initial eld value $\varphi(0)$, the approach we take is to search for the ground state eigenfrequency ω_0 of a boson star via a shooting method. Alternatively, one could also take the approach of xing the eigenfrequency ω_0 and searching for the corresponding initial eld value $\varphi(0)$. However, for the purposes of our project, the former approach makes it easier to nd the desired thin-wall stars.

The shooting method we use is predicated on the observation that near the eigenfrequencies ω_n, the dominant exponentially growing mode of the solution of the di erential eqs. (2.7) for the star will diverge either upwards or downwards depending on whether our value of ω is larger or smaller than ω_n. Because of this divergence, it is possible to perform a binary search in the variable ω to tune it as arbitrarily close to ω_n as allowed by machine precision.

This is done roughly as follows: if we have a range $[a, b]$ that includes the desired eigenfrequency ω_0 and is also su ciently small, then nding ω_0 is simply a matter of binary search { that is, we test the midpoint $(a + b)/2$ by integrating the di erential eqs. (2.7) for the star outwards, check the direction in which the result diverges and then replace $[a, b]$ with either $[a, (a + b)/2]$ or $[(a + b)/2, b]$, depending on which we believe the eigenfrequency ω_0 lies in. We repeat this procure until we are su ciently happy with the result, which is normally when the solution to (2.7) no longer diverges in some region $[0, R_{\text{max}}]$.

However, we will in general not be handed a sufficiently small range $[a, b]$ in which to perform the search, so we must contend with the situation where the range $[a, b]$ may include other eigenfrequencies $\omega_1, \omega_2, \ldots$. This situation can be addressed using the fact that the excited states of the boson star usually exhibit a zero in their profile $\varphi(r)$. Indeed, the profile $\varphi_n(r)$ corresponding to the eigenfrequency ω_n usually exhibits n zeroes. Thus, if we check the number of zeroes of the solution to (2.7) we can tell whether we are near an excited eigenfrequency rather than the ground frequency and correct accordingly. Written out, the full algorithm is shown below.

Algorithm 1 Computing ground states of boson stars on a region $[0, R]$

procedure COMPUTEGROUNDSTATE(φ_0) ▷ Compute ω_0 and $\varphi(r)$ for a given $\varphi(0)$
  $(\omega_{\text{min}}, \omega_{\text{max}})$ COMPUTERANGEGUESS(φ_0)
  $\varphi(r)$ *1* ▷ Initialize profile function $\varphi(r)$ to infinity
  while φ is divergent or $|\varphi(R)| > \epsilon$ **do** ▷ ϵ is an arbitrary small constant
    ω $(\omega_{\text{min}} + \omega_{\text{max}})/2$
    $\varphi(r)$ SOLVEEQUATIONS(φ_0, ω) ▷ Details in sections 2.1.1 and 2.1.2
    n NUMBEROFZEROES(φ)
    if $n > 0$ **then**
      $(\omega_{\text{min}}, \omega_{\text{max}})$ $(\omega_{\text{min}}, \omega)$ ▷ Search lower
    else if φ diverges upwards **then**
      $(\omega_{\text{min}}, \omega_{\text{max}})$ $(\omega, \omega_{\text{max}})$ ▷ Search higher
    else if φ diverges downwards **then**
      $(\omega_{\text{min}}, \omega_{\text{max}})$ $(\omega_{\text{min}}, \omega)$ ▷ Search lower
    else if $\varphi(R) > 0$ **then**
      $(\omega_{\text{min}}, \omega_{\text{max}})$ $(\omega, \omega_{\text{max}})$ ▷ Search higher
    else if $\varphi(R) < 0$ **then**
      $(\omega_{\text{min}}, \omega_{\text{max}})$ $(\omega_{\text{min}}, \omega)$ ▷ Search lower
    end if
  end while
  return (ω, φ)
end procedure

As one can see, the algorithm first looks for solutions with no zeroes (i.e. those in the vicinity of the ground state eigenfrequency ω_0). Then, it performs a binary search based on which way the profile $\varphi(r)$ diverges, and once $\varphi(r)$ no longer diverges in the integration region $[0, R]$, the algorithm attempts to get $\varphi(R)$ close to 0. To prevent the algorithm from running for an arbitrarily long time, we place an iteration constraint upon the loop,

so it terminates within a certain number of steps. Some implementation details worth mentioning:

1. ComputeRangeGuess: this function computes an initial guess for the range in which the eigenfrequency ω_0 lies. The size of the search range diminishes exponentially with iteration, so there is no problem starting the iteration with a large initial range. In our code, we use the initial range $[m/10, 20m]$.

2. NumberOfZeroes: counts the number of times $\varphi(r)$ crosses zero.

3. Divergence of $\varphi(r)$: we designate a threshold for $|\varphi(r)|$ to determine when divergence occurs. The threshold we use is $2\varphi(0)$.

Important Note on Precision: In practice, 64-bit floating-point precision is sometimes insufficient to come adequately close to the ground state frequency ω_0 such that the corresponding solution $\varphi(r)$ becomes apparent. For mini-boson stars and massive boson stars, the above algorithm can be implemented with 64-bit precision. From our experience, the solutions for these stars emerge before the limits of 64-bit precision are exhausted. However, this is not the case for the ground states of solitonic boson stars, particularly when concerning the thin-wall solutions we are primarily interested in. Because the solutions of solitonic boson stars are often extremely sensitive to changes in ω, it is necessary to use high-precision arithmetic if one wishes to have any hope of being able to recover the desired ground states. We recommend using at least 256-bit precision. Our code uses the software package GMP to implement high-precision computations in software, and the examples we will show in the subsequent section were computed using 512-bit floating point precision. Although the loss of hardware acceleration in floating point computations means the performance of the algorithm does take a significant hit, the algorithm still performs well enough that it allows us to compute solutions in very reasonable times on relatively modest hardware, especially if one optimizes the SolveEquations procedure to terminate early when the divergence

threshold has been reached.

2.2 Results and Observations

In this section, we give a brief overview of the results of our computations described in the first half of this chapter. All of the values given are in natural units $\hbar = G = c = 1$. We also note briefly that we have checked convergence of our results with resolution, although there is not a section in this chapter dedicated to this. A further discussion of convergence can be found in section 3.1.5.

2.2.1 Ground States of Mini and Massive Boson Stars

In general, the ground states of mini and massive boson stars we observed using our algorithm have profiles which appear approximately Gaussian. For mini-boson stars, in the sector of fixed mass m, there is generally a maximum and minimum threshold of the initial field value $\varphi(0)$ for which it is possible to find ground states. In figure 2.1, we see the profile functions $\varphi(r)$ plotted for a mini-boson star with $m = 1$ and $\kappa = 8\pi$ at different central densities $\varphi(0)$.

Note, as the central density decreases, the radius of the star decreases and the star becomes more compact. This trend can also be seen in the table 2.1 below, where we list the salient properties of each of the stars seen in figure 2.1. The mass M is defined in (1.52). Here, the radius R of the boson star is defined as the radius of the sphere which contains 99% of the mass of the star.

$\varphi(0)$	Frequency (ω)	Mass (M)	Radius (R)	Compactness (R/M)
0.015	1.0531	0.4845	16.67	34.37
0.03	1.1160	0.5919	11.28	19.06
0.05	1.2190	0.6321	8.26	13.07
0.1	1.6244	0.5697	5.29	9.28
0.15	2.4480	0.4530	4.24	9.36

Table 2.1: Properties of mini-boson stars at different central densities with mass $m = 1$

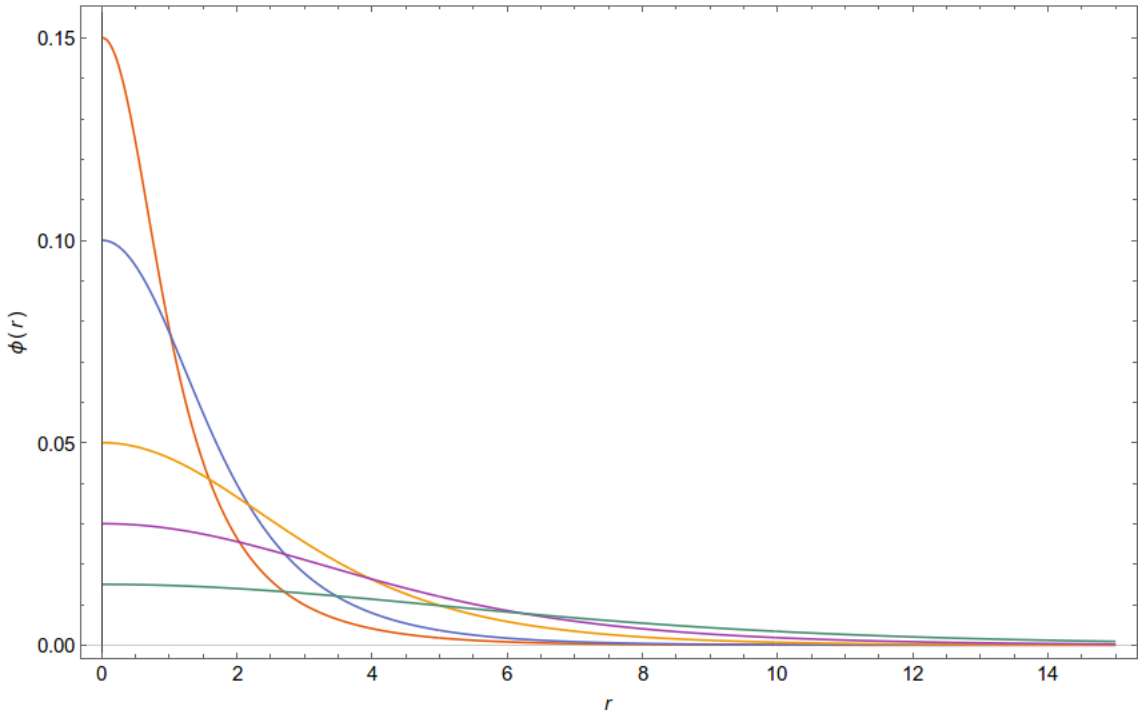

Figure 2.1: Field pro les for mini-boson stars at di erent central densities with mass m = 1.

Depending on the value of the parameter λ, the ground states of massive boson stars exhibit more or less the same features, except they tend to have higher mass for a given value of $\varphi(0)$. Examples can be seen in gure 2.2 and the corresponding properties of the stars in table 2.2.

$\varphi(0)$	Frequency (ω)	Mass (M)	Radius (R)	Compactness (R/M)
0.015	1.0586	0.5374	16.72	31.17
0.03	1.1393	0.6935	11.24	16.21
0.05	1.2886	0.7563	8.14	10.76
0.1	1.9322	0.6276	5.21	8.30
0.15	3.1859	0.4661	4.62	9.91

Table 2.2: Properties of massive boson stars di erent central densities with mass m = 1 and self interaction term λ = 100.

We computed all results in this section with standard 64-bit oating point precision.

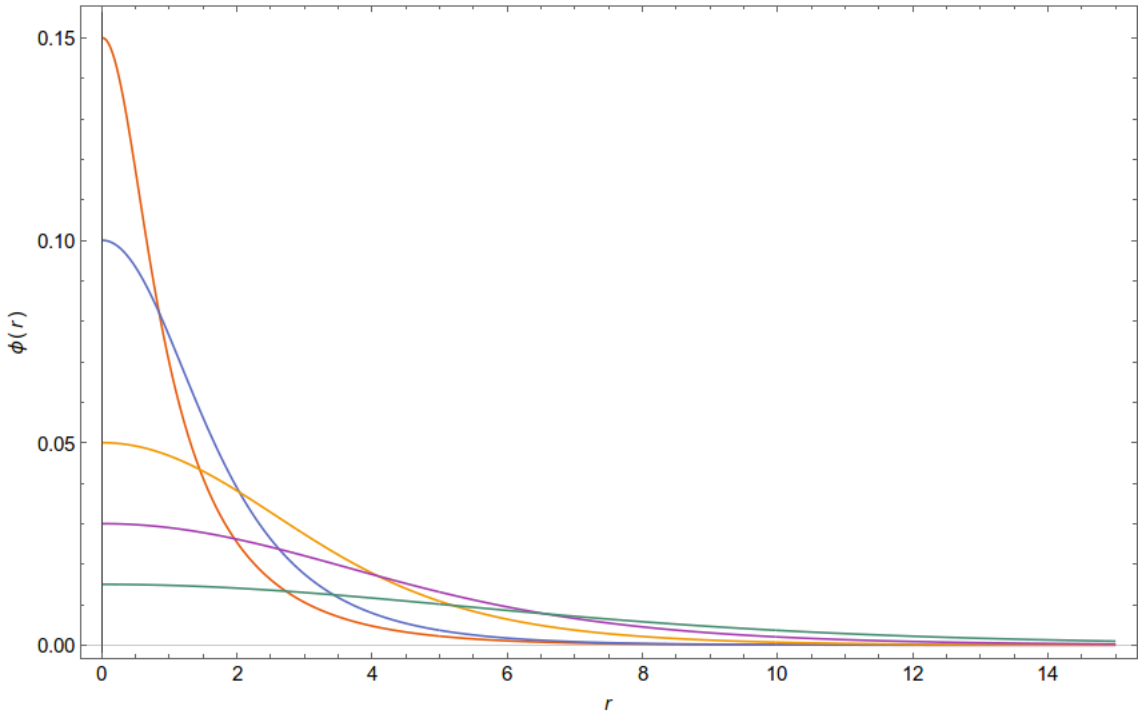

Figure 2.2: Field pro les for massive boson stars at di erent central densities with mass m = 1 and self interaction term λ = 100

2.2.2 Ground States of Solitonic Boson Stars

The ground states of solitonic boson stars are somewhat more interesting than the states observed in the previous section. To begin, we were able to observe the desired thin-wall ground state under certain conditions. While these states deviate considerably from those observed for mini and massive boson stars, it is still possible to obtain ground states of solitonic boson stars that posses the same Gaussian-like pro le as their mini and massive counterparts. Indeed, there seems to be a critical value at which the thin-wall static solution to the ordinary di erential equations becomes available and this threshold occurs very slightly above (or perhaps at) the degenerate vacuum level σ of the solitonic boson star. It seems fairly clear that this degenerate vacuum is the di erentiating factor which allows these thin-wall ground states to form.

In gure 2.3, we can see a number of di erent pro les of the ground states of solitonic boson stars at di erent central eld densities. The orange pro le corresponds to our desired

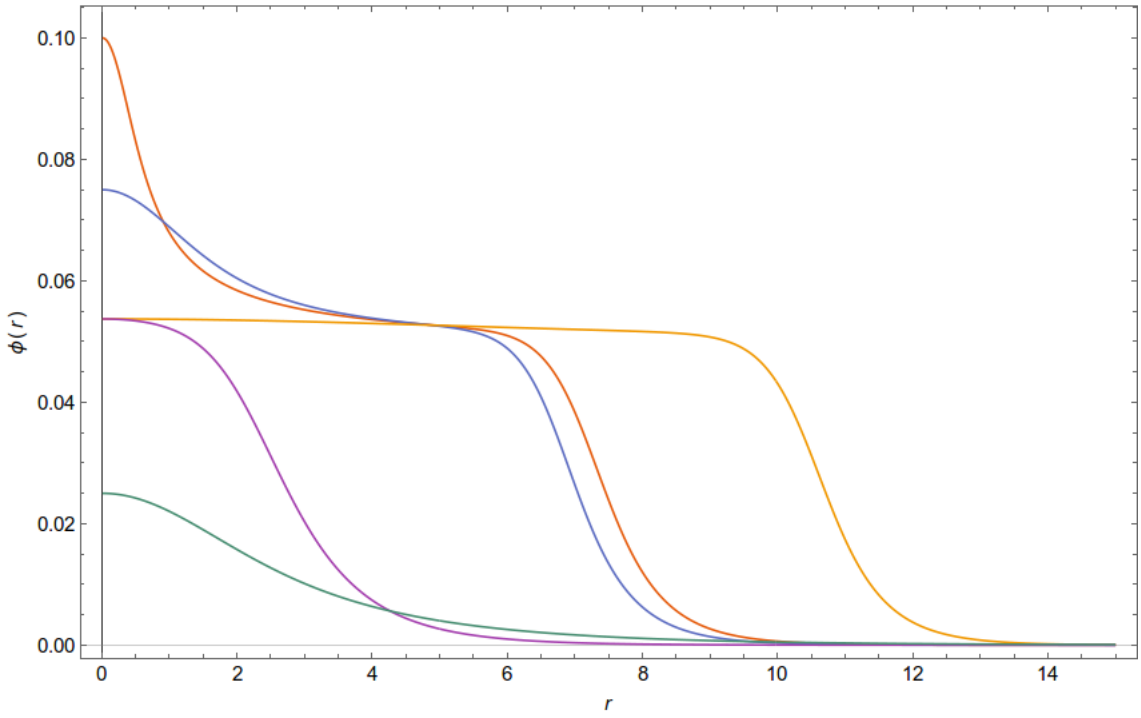

Figure 2.3: Field pro les for solitonic boson stars with mass m = 1 and degenerate vacuum parameter σ = 0.05. Note how pro les which start above the degenerate vacuum σ = 0.05 tend to plateau near σ. Otherwise, solitonic boson stars whose central eld density is below σ have very similar pro les to those of mini and massive boson stars. An example thin-wall ground state can be seen in the orange pro le. Note also the abrupt transition which occurs in the pro le of the solitonic boson stars near central density $\varphi(0)$ 0.0537.

thin-wall state. This state is reasonably compact at R/M 3.5 and has a shell-like mass distribution, since the interior essentially consists of a vacuum. The mass of the star is primarily found in the transition of the pro le from the degenerate vacuum at σ to the true vacuum. This transition happens in the range 10 r 12. In general, ground states that have central eld densities signi cantly above σ will plateau near the degenerate vacuum before they transition to the true vacuum. Strangely, there is a very abrupt transition between thin-wall ground states (orange) and ground states that resemble the Gaussian-like ground states of the mini and massive boson stars we examined earlier (purple) around $\varphi(0)$ 0.0537. In fact, the transition is amazingly sudden { for reference, the orange pro le has central eld density $\varphi(0)$ = 0.053720782161578 and the purple pro le has central eld density $\varphi(0)$ = 0.053720782161577. The extent of the di erence between the two states can

be seen in table 2.3.

$\varphi(0)$	Freq. (ω)	Mass (M)	Radius (R)	Compactness (R/M)
0.01	1.0117	0.1529	18.88	123.50
0.025	**0.9952**	**0.1006**	**10.14**	**100.82**
0.03	0.9833	0.0931	8.67	93.06
0.05	0.8527	0.1138	5.36	46.99
0.053720782161577	**0.7176**	**0.2065**	**5.26**	**25.48**
0.053720782161578	**0.6215**	**3.4060**	**11.79**	**3.46**
0.075	**2.7961**	**2.1858**	**8.04**	**3.68**
0.1	**6.2834**	**2.2617**	**8.50**	**3.76**
0.15	18.1198	2.3572	8.63	3.66

Table 2.3: Properties of solitonic boson stars at di erent central densities with mass m = 1 and degenerate vacuum parameter σ = 0.05. The boson stars marked in bold are shown in gure 2.3.

Bizarrely, the reason for the jump between very di erent pro les lies in the strange behavior of the equations in a very small range of central densities above the degenerate vacuum level. For central densities in the approximate range 0.05 to 0.053, there are actually *two* ground states, one corresponding to the Gaussian-like pro le and the other corresponding to the thin-wall pro le. Although the thin-wall ground state in this central density range has a lower eigenfrequency ω_0 than the Gaussian-like state, in practice, the algorithm of the previous section fails to nd these states because the equations diverge in the same direction in the vicinity of the eigenfrequency ω_0. As a result, these ground states are e ectively hidden and the algorithm instead favors the Gaussian-like \ground states" with higher frequency.

However, with knowledge of a small enough interval $[\omega_{\text{min}}, \omega_{\text{max}}]$ containing ω_0 and no other eigenfrequencies, it is fairly simple to modify the algorithm to nd the thin-wall ground state by changing criteria used as the basis for the binary search. Instead of checking the direction in which the solution diverges, we check whether the pro le is below or above zero before the solution diverges. Using this modi cation, we have veri ed that such thin-wall ground states exist even below $\varphi(0)$ 0.053. They are slightly more compact, and hence, are the desired objects for studying the stability of these ground states in chapter 3.

2.2.3 Unit Conversion

In the above calculations, we have used natural units $c = G = \sim = 1$. For a mass parameter of $m = 1$, these correspond to Planck Units. In these units, all quantities expressible in terms of length L, time T, and mass M are dimensionless. In standard units, the relationship between length, time, and mass is given by the dimensions

$$[c] = \frac{L}{T} \qquad \left[\frac{G}{c^2}\right] = \frac{L}{M} \tag{2.16}$$

Therefore, the conversion factor from time to length is c and the conversion factor from mass to length is G/c^2. Moreover, the fundamental length scale of Planck units is the Planck length $l_p = \sqrt{G\sim/c^3}$, and every length in Planck units is expressed as a dimensionless multiple of the this length l_p. A conversion between Planck units and standard units now entails the following: one first uses the relationship (2.16) to convert all quantities to dimensions of length, and then converts the resulting length-based quantities to standard units using the Planck length l_p. Given a quantity which has nongeometrized dimensions $L^n T^m M^p$, the conversion factor to geometrized units is $c^m (G/c^2)^p$, and from there, the conversion factor to Planck units is l_p^{n+m+p}. The following table provides a reference of pre-computed conversion factors:

Quantity	Dimension	Conversion Factor	Fundamental Scale
Length	L	l_p	$1.6 \quad 10^{-35}$ m
Time	T	cl_p	$5.4 \quad 10^{-44}$ s
Mass	M	Gl_p/c^2	$2.2 \quad 10^{-5}$ g
Energy	$L^2T^{-2}M$	Gl_p/c^4	$1.3 \quad 10^{19}$ GeV
Mass density	$L^{-3}M$	$G/c^2l_p^2$	$5.2 \quad 10^{99}$ g m^{-3}
Energy density	$L^{-1}T^{-2}M$	$G/c^4l_p^2$	$3.2 \quad 10^{123}$ GeV m^{-3}

Table 2.4: Conversion factors from Planck units to standard units.

Chapter 3

Solitonic Boson Star Perturbations

In this second part of the project, we endeavor to build a numerical code to simulate the evolution of a thin-wall solitonic boson star perturbed by a small amount of incoming scalar radiation. Once again, this chapter is split into two sections. In the first section, we give details about the implementation of the numerical code { ranging from the underlying form of Einstein's equations and the Klein-Gordon equations we used, to their discretization and evolution using finite differences. In the second section, we give results of our simulations and observations. As laid out in the introduction, our overarching goal is to determine whether the thin-wall ground states from chapter 2 are stable with respect to small perturbations. Indeed, if they are not, then it would most likely be infeasible to mimic the gravitational signal GW150914.

3.1 Algorithm for Numerical Evolution

Here we give an outline of the evolution code we use to produce simulations of solitonic boson stars perturbed by a small amount of incoming scalar radiation, in a similar manner to the evolution code of Hawley and Choptuik, which we have described to an extent in section 1.3.2. The primary difference between our code and the one used by Hawley and Choptuik is that we use a different gauge condition for our coordinate system. Instead of the *geodesic slicing* condition, where the shift vector β is equal to zero, we use the *maximal*

slicing condition, where the trace of the extrinsic curvature is forced to be zero,

$$K^{\mu}{}_{\mu} = 0 . \tag{3.1}$$

For a quick overview of extrinsic curvature, please see appendix A. Furthermore, we again restrict ourselves to spherical symmetry and let the spatial metric be given in *isotropic* form,

$$ds^2 = -(\alpha^2 - \psi^4\beta^2)\,dt^2 + 2\psi^4\beta\,dr\,dt + \psi^4(dr^2 + r^2\,d\Omega^2) . \tag{3.2}$$

The most important difference between this metric and the one seen in section 1.3.2 is the presence of a shift β which will generally be nonzero. Together, the gauge conditions (3.1) and (3.2) will be sufficient to fully specify the evolution of our system. The system itself is a carbon copy of what we examined in section 1.3.2, except now the potential $V(|\nabla\Phi_C|^2)$ is allowed to be arbitrary. For the benefit of the reader, we list the underlying equations here again with slight modification. We have the Einstein-Hilbert action

$$S = \int_M \left[\frac{1}{2\kappa}R + \mathcal{L}_C(\Phi_C, \nabla\Phi_C) + \mathcal{L}_R(\Phi_R, \nabla\Phi_R)\right]\sqrt{-g}\,d^4x , \tag{3.3}$$

where the individual Lagrangian densities $\mathcal{L}_C$ and $\mathcal{L}_R$ for the fields Φ_C and Φ_R are given by

$$\begin{aligned} \mathcal{L}_C(\Phi_C, \nabla\Phi_C) &= -\nabla^{\mu}\Phi_C\,\nabla_{\mu}\Phi_C - V(|\nabla\Phi_C|^2) , \\ \mathcal{L}_R(\Phi_R, \nabla\Phi_R) &= -\nabla^{\mu}\Phi_R\,\nabla_{\mu}\Phi_R . \end{aligned} \tag{3.4}$$

The resulting Einstein equations are

$$R_{\mu\nu} - \frac{1}{2}g_{\mu\nu}R = \kappa(T^C_{\mu\nu}(\Phi_C) + T^R_{\mu\nu}(\Phi_R)) , \tag{3.5}$$

where the stress-energy tensors $T^C_{\mu\nu}$ and $T^R_{\mu\nu}$ are given by

$$\begin{aligned} T^C_{\mu\nu}(\Phi_C) &= \nabla_{\mu}\Phi_C\,\nabla_{\nu}\Phi_C + \nabla_{\mu}\Phi_C\,\nabla_{\nu}\Phi_C - g_{\mu\nu}(\nabla_{\rho}\Phi_C\,\nabla^{\rho}\Phi_C + V(|\nabla\Phi_C|^2)) , \\ T^R_{\mu\nu}(\Phi_R) &= 2\nabla_{\mu}\Phi_R\,\nabla_{\nu}\Phi_R - g_{\mu\nu}\nabla_{\rho}\Phi_R\,\nabla^{\rho}\Phi_R . \end{aligned} \tag{3.6}$$

And finally, the Klein-Gordon equations governing the motion of the fields are given by

$$\begin{aligned} \nabla_{\mu}\nabla^{\mu}\Phi_C &= \frac{dV}{d|\nabla\Phi_C|^2}\Phi_C , \\ \nabla_{\mu}\nabla^{\mu}\Phi_R &= 0 . \end{aligned} \tag{3.7}$$

Once again, we introduce the auxiliary variables to reduce the Klein-Gordon equations to first order form. Note that they are slightly different this time due to the change in metric.

$$\begin{aligned} \xi_1 \quad & {}^{0}_{1}, \quad {}_{1} \quad \frac{\psi^2}{\alpha}\left(- {}_{1} \quad \beta\xi_1 \right), \\ \xi_2 \quad & {}^{0}_{2}, \quad {}_{2} \quad \frac{\psi^2}{\alpha}\left(- {}_{2} \quad \beta\xi_2 \right), \\ \xi_3 \quad & {}^{0}_{3}, \quad {}_{3} \quad \frac{\psi^2}{\alpha}\left(- {}_{3} \quad \beta\xi_3 \right). \end{aligned} \tag{3.8}$$

We can now derive a number of elliptic constraints for the metric variables ψ, β, α as well as a set of hyperbolic equations for the variables $\xi_1, \xi_2, \xi_3, \ {}_1, \ {}_2, \ {}_3$ that will be used to evolve initial data. If we begin with the maximal slicing condition (3.1) and expand it in terms of the metric variables, we arrive at

$$\psi \quad \beta\left(\frac{\psi}{3r} + \psi^{0} \right) \quad \frac{\psi\beta^{0}}{6} = 0. \tag{3.9}$$

This equation will be used to replace time derivatives of ψ with spatial derivatives in the variables ψ and β in subsequent derivations. Indeed, one can use eq. (3.9), as well as relevant substitutions from the definitions (3.8), to expand the set of three Klein-Gordon equations into hyperbolic evolution equations for the variables ${}_k$,

$$- {}_k \quad \frac{1}{r^2\psi^4}\left[r^2\psi^4\left(\beta \ {}_k + \frac{\alpha\xi_k}{\psi^2} \right) \right]^{0} + \frac{2}{3} \ {}_k \left[\beta^{0} + \frac{2\beta}{r}\left(1 + \frac{3r\psi^{0}}{\psi} \right) \right] = \alpha\psi^2 \frac{dV}{d\mathbf{j}_{\ C}\mathbf{j}^2} \ {}_k(1 \quad \delta_{3k}), \tag{3.10}$$

for $k = 1, 2, 3$. The hyperbolic evolution equations for the variables ξ_k are easily derived from the definitions (3.8) of the auxiliary variables, yielding

$$\xi_k = \left(\frac{\alpha \ {}_k}{\psi^2} + \beta\xi_k \right)^{0}. \tag{3.11}$$

To obtain elliptic equations for the variables ψ, α, and β, we first define the tensor

$$X_{\mu\nu} \quad R_{\mu\nu} \quad \frac{1}{2}g_{\mu\nu}R \quad \kappa T^{C}_{\mu\nu}(\ {}_C) \quad \kappa T^{R}_{\mu\nu}(\ {}_R). \tag{3.12}$$

The Einstein eqs. (3.5) can then be used to write

$$X^{\mu\nu}n_\mu n_\nu = 0, \tag{3.13}$$

where $n_\mu = \alpha\, dt$ is the dual of the normal vector of our foliation (see appendix A for more details). Expanding the above equations and using the same substitutions which were used to derive (3.10), we arrive at *Hamiltonian constraint equation*, our elliptic constraint equation for the field variable ψ,

$$\psi'' + \frac{2\psi'}{r} + \frac{\psi^5}{12}\left[\frac{1}{\alpha}\left(\beta' - \frac{\beta}{r}\right)\right]^2 + \frac{1}{4}\kappa\psi\left[\xi_1^2 + \xi_2^2 + \xi_3^2 + \pi_1^2 + \pi_2^2 + \pi_3^2 + \psi^4 V(\pi_1^2 + \pi_2^2)\right] = 0. \tag{3.14}$$

The elliptic eq. (3.14) now gives a way to eliminate ψ'' terms in subsequent derivations. To derive an elliptic equation for the variable β, we use the identity

$$X_{00} - \beta X_{10} = 0. \tag{3.15}$$

Expanding the identity above and then using the relevant substitutions from (3.8), (3.9), and (3.14) results in our desired elliptic constraint equation for β, the *momentum constraint*,

$$\beta'' + \left(\beta' - \frac{\beta}{r}\right)\left(\frac{2}{r} + \frac{6\psi'}{\psi} - \frac{\alpha'}{\alpha}\right) + \frac{3\kappa\alpha}{\psi^2}(\xi_1\pi_1 + \xi_2\pi_2 + \xi_3\pi_3) = 0. \tag{3.16}$$

Once again, this allows us to eliminate any β'' terms in subsequent equations. Now, for the final elliptic equation in our system, we use the following identity:

$$X_{44} + \frac{r^2}{2}X_{33} = 0, \tag{3.17}$$

which, when applying all relevant substitutions from the prior eqs. (3.8), (3.9), (3.14), and (3.16), gives us the final elliptic constraint equation for the variable α:

$$\alpha'' + \alpha'\left(\frac{2}{r} + \frac{2\psi'}{\psi}\right) - \frac{1}{\alpha}\left[\frac{2\psi^4}{3}\left(\beta' - \frac{\beta}{r}\right)^2\right] - 2\kappa\alpha\left(\pi_1^2 + \pi_2^2 + \pi_3^2\right) + \kappa\alpha\psi^4 V(\pi_1^2 + \pi_2^2) = 0. \tag{3.18}$$

The eqs. (3.10), (3.11), (3.14), (3.16), (3.18) together with the definitions of π_1, π_2, π_3 form a closed system for the variables $\{\pi_1, \pi_2, \pi_3, \xi_1, \xi_2, \xi_3, \pi_1', \pi_2', \pi_3', \alpha, \beta, \psi\}$, which we use as the basis for our evolution scheme. Note that, for the purposes of evolution, the constraint eq. (3.18) can in principle be replaced by the hyperbolic evolution eq. (3.9), since the two are essentially equivalent. These equations can now be solved using a finite difference scheme.

However, first we must specify boundary conditions on the ends of the region $[0, R]$ where we want to solve the equations. At the origin, this is fairly easy, spherical symmetry demands that we have Neumann conditions for ψ, α, and $_k$, i.e.,

$$\psi^{\prime}(0) = 0\,, \qquad \alpha^{\prime}(0) = 0\,, \qquad {}^{\prime}_{k}(0) = 0\,. \tag{3.19}$$

Spherical symmetry also imposes Dirichlet conditions for β and ξ_k at the origin, i.e.,

$$\beta(0) = 0\,, \qquad \xi_k(0) = 0\,. \tag{3.20}$$

As for the boundary conditions at the opposite end of the computation region $[0, R]$, assuming that R is very large, we want the metric to become approximately Minkowski as $r \;!\; R$. Hence, we impose the conditions

$$\psi(R) = 1\,, \qquad \alpha(R) = 1\,, \qquad \beta(R) = 0\,. \tag{3.21}$$

Thus, for very large r, the Klein-Gordon equations governing the system essentially become (massive/massless) wave equations on R. This means it makes sense to enforce decoupled outgoing Sommerfeld radiation conditions at $r = R$, i.e.,

$$\xi_k(R) = \quad \xi^{\prime}_k(R)\,, \qquad {}_{-k}(R) = \quad {}^{\prime}_{k}(R)\,. \tag{3.22}$$

And since $_k$ are obtained via the definitions of $_k$, we do not need explicit boundary conditions for them.

The system is evolved numerically using an iterative scheme at each time step. During each step, we alternate between updates of the variables ξ_k and $_k$ described later in section 3.1.1, updates of the variables α, β, ψ described in section 3.1.2, and updates of the variables $_k$ described in section 3.1.3. These updates iterate until we reach convergence. When convergence is reached, the algorithm proceeds to the next time step.

To discretize the continuous system above, we use second order finite differences. Specifying some spatial spacing r and some temporal spacing t, we store and compute samples of the underlying variables at the grid points $(r, t) = (i \;\; r, j \;\; t)$ for $i, j \; 2 \; \mathbb{Z}_{\;0}$ and we will denote these samples using the notation $F^{j}_{i} \quad F(r, t)$. Now, we replace the continuous

derivative operators in the equations by discrete nite di erence approximations. For the elliptic equations, the continuous derivative operators ∂_r, ∂_r^2 now become the nite di erence operators δ_r, δ_r^2, which we de ne as

$$\begin{aligned} \delta_r[F](r,t) &\quad \frac{F(r+\quad r,t)\quad F(r\qquad r,t)}{2\quad r}, \\ \delta_r^2[F](r,t) &\quad \frac{F(r+\quad r,t)\quad 2F(r,t)+F(r\qquad r,t)}{(\quad r)^2}. \end{aligned} \tag{3.23}$$

The time derivative ∂_t becomes the backwards nite di erence operator r_t in time,

$$r_t[F](r,t) \quad \frac{F(r,t)\quad F(r,t\qquad t)}{t}. \tag{3.24}$$

The boundary conditions (3.20) use the spatial forward di erence operator. The spatial forward di erence operator is de ned as

$$_r[F](r,t) \quad \frac{F(r+2\quad r,t)+4F(r+\quad r,t)\quad 3F(r,t)}{2\quad r}. \tag{3.25}$$

Likewise, the boundary conditions (3.22) use the spatial backwards di erence operator,

$$r_r[F](r,t) \quad \frac{F(r\quad 2\quad r,t)\quad 4F(r\qquad r,t)+3F(r,t)}{2\quad r}. \tag{3.26}$$

3.1.1 Update Method for the Hyperbolic Equations

Since the hyperbolic eqs. (3.10) and (3.11) exhibit nite speed of propagation, it su ces to update the variables $\xi_k, \quad _k$ by using successive replacement. First, let us discretize the eqs. (3.10) and (3.11) using the spatial nite di erence operators in (3.23) and the time nite di erence operator in (3.24). Let $\boldsymbol{Y}$ be the vector of all of the variables $f \quad _1, \quad _2, \quad _3, \xi_1, \xi_2, \xi_3, \quad _1, \quad _2, \quad _3, \alpha, \beta, \psi g$ and let $\boldsymbol{Y}^j$ denote the vector at time index j. First, write the eqs. (3.10) and (3.11) in the form

$$\begin{aligned} \xi_k &= L^{\xi_k}[\boldsymbol{Y}], \\ \_k &= L\quad ^k[\boldsymbol{Y}]. \end{aligned} \tag{3.27}$$

Then using the Crank-Nicolson method, we can discretize L using nite di erences and rewrite (3.27) as

$$\begin{aligned} r_t\xi_k &= \frac{1}{2}L^{\xi_k}[\boldsymbol{Y}^j]+\frac{1}{2}L^{\xi_k}[\boldsymbol{Y}^j\quad ^1], \\ r_t\quad _k &= \frac{1}{2}L\quad ^k[\boldsymbol{Y}^j]+\frac{1}{2}L\quad ^k[\boldsymbol{Y}^j\quad ^1], \end{aligned} \tag{3.28}$$

where L^{ξ_k} and $L^{\ k}$ are the discrete versions of the di erential operators L^{ξ_k} and $L^{\ k}$. L^{ξ_k} and $L^{\ k}$ result from replacing the derivative operators in (3.10) and (3.11) with their nite di erence approximations. Note the time index j is suppressed on the left-hand side, and on the right, we apply Crank-Nicolson and take the average of the operator at time j and time $j \quad 1$ for better stability. An update for the interior of the region $[0, R]$ is now done via successive replacement. Solving (3.28) for $(\xi_k)_i^j$ and $(\ _k)_i^j$, respectively, gives

$$\begin{aligned}(\xi_k)_i^j &= \frac{t}{2} L_i^{\xi_k}[\boldsymbol{Y}^j] + \frac{t}{2} L_i^{\xi_k}[\boldsymbol{Y}^{j\ 1}] + (\xi_k)_i^{j\ 1}, \\ (\ _k)_i^j &= \frac{t}{2} L_{i\ }^{\ k}[\boldsymbol{Y}^j] + \frac{t}{2} L_{i\ }^{\ k}[\boldsymbol{Y}^{j\ 1}] + (\ _k)_i^{j\ 1}.\end{aligned} \tag{3.29}$$

Updating the $(\xi_k)_i^j$'s is now accomplished by iterating through $i = 1, 2, ..., N \quad 2$ (where N is the number of grid points) and performing the following replacement:

$$\begin{aligned}(\xi_k)_i^j &\quad \frac{t}{2} L_i^{\xi_k}[\boldsymbol{Y}^j] + \frac{t}{2} L_i^{\xi_k}[\boldsymbol{Y}^{j\ 1}] + (\xi_k)_i^{j\ 1}, \\ (\ _k)_i^j &\quad \frac{t}{2} L_{i\ }^{\ k}[\boldsymbol{Y}^j] + \frac{t}{2} L_{i\ }^{\ k}[\boldsymbol{Y}^{j\ 1}] + (\ _k)_i^{j\ 1}.\end{aligned} \tag{3.30}$$

In the same way, we discretize the boundary condition (3.20) at $i = 0$ and the boundary condition (3.22) at $i = N \quad 1$, except these boundary conditions use the the forward and backwards Crank-Nicolson di erence operators (3.25) and (3.26), respectively. Note that replacement is is done in increasing order of i, that is, starting at $i = 0$ and ending at $i = N \quad 1$. If our initial guesses for $(\xi_k)_i^j$ and $(\ _k)_i^j$ are close enough to the solution of (3.28), as they are in practice, then multiple iterations of (3.30) will converge quickly to the solution of (3.28), which is a xed point of (3.30).

3.1.2 Update Method for the Elliptic Equations

The update method for the elliptic equations is somewhat more involved, as we use a Newton-Gauss-Seidel relaxation to update the variables $\{\alpha, \beta, \psi\}$. Since the method does not consider data from previous times, we will drop all superscripts denoting time in this section. As an illustrative example, consider the eld ψ. First, write eq. (3.14) in terms of a di erential operator L, i.e.,

$$L[\psi] = 0. \tag{3.31}$$

From L, we create a finite difference operator L such that

$$L_i[\psi] = 0\,, \tag{3.32}$$

where L_i is the discretized form of L for grid points $i = 1, 2, ..., N-2$, $L_0[\psi] = 0$ gives the boundary condition $\psi'(0) = 0$, and $L_{N-1}[\psi] = 0$ gives the boundary condition $\psi(R) - 1 = 0$. Assume that we have some guess $\hat{\psi}$ of what the true solution to the system of eqs. (3.32) should be, so that our guess and the true solution differ by a small error term ϵ,

$$\psi = \hat{\psi} + \epsilon\,. \tag{3.33}$$

Because ϵ is small, we may Taylor expand $L_i[\hat{\psi} + \epsilon] = 0$ in the variable ϵ, to obtain

$$L_i[\hat{\psi}] + \sum_j \frac{\partial L_i}{\partial \psi_j}\epsilon_j + O(\epsilon^2) = 0\,. \tag{3.34}$$

We define the *Jacobian* matrix J_{ij} as

$$J_{ij}[\hat{\psi}] \equiv \frac{\partial L_i}{\partial \psi_j}\,. \tag{3.35}$$

The *residual* vector R_i is defined as

$$R_i[\hat{\psi}] \equiv -L_i[\hat{\psi}]\,. \tag{3.36}$$

Ignoring higher order terms in ϵ, (3.34) can be rewritten as a matrix equation,

$$\vec{R} + J\vec{\epsilon} = 0\,, \tag{3.37}$$

from which we can compute the error vector $\vec{\epsilon}$,

$$\vec{\epsilon} = -J^{-1}\vec{R}\,. \tag{3.38}$$

For our applications, the discrete differential operator L_i acts only locally and hence the corresponding Jacobian J_{ij} is very sparse. Indeed, J_{ij} is nearly tridiagonal except for two entries on the top and bottom rows. Thus, the linear system of eqs. (3.38) can be solved via a banded or sparse matrix solver. Our code uses the Eigen linear algebra library and

performs a sparse LU decomposition to compute $\vec{\epsilon}$. Once we have the error, we can update ψ,

$$\psi \quad \psi + \epsilon . \tag{3.39}$$

Note that since we have dropped $O(\epsilon^2)$ terms in making this approximation, the solution obtained is not exact unless L is a linear operator. Thus, one should iterate the Newton-Gauss-Seidel procedure until the residual $L_i[\hat{\psi}]$ is su ciently small. In our code, the same exact procedure is applied to the variables α and β, but the relaxations of α, β, and ψ are staggered with the other updates: we perform a relaxation for α, then a relaxation for β, and then a relaxation for ψ, repeating until we have convergence.

3.1.3 Update Method for the Scalar Fields

The update method for the scalar elds $_1$, $_2$, $_3$ is essentially identical to those in section 3.1.1. However, in this case, the underlying equations are taken from the de nitions (3.8) of $_k$. Rewriting these provides

$$-_k = \frac{\alpha}{\psi^2} \; _k + \beta\xi_k . \tag{3.40}$$

We again discretize this equation using the Crank-Nicolson method, and nd the corresponding update rule, which results in

$$(\;_k)_i^j \quad \frac{t}{2}\left(\frac{\alpha_i^j}{(\psi_i^j)^2}(\;_k)_i^j + \beta_i^j(\xi_k)_i^j\right) + \frac{t}{2}\left(\frac{\alpha_i^{j\;1}}{(\psi_i^{j\;1})^2}(\;_k)_i^{j\;1} + \beta_i^{j\;1}(\xi_k)_i^{j\;1}\right) + (\;_k)_i^{j\;1} . \tag{3.41}$$

3.1.4 The Full Algorithm

Putting together all the update steps of sections 3.1.1, 3.1.2, and 3.1.3, we obtain a full algorithm for performing a numerical evolution for some given set of initial data $\boldsymbol{Y}^0$. For each time step of the evolution, we continually perform interlaced updates of the all of the variables as detailed in sections 3.1.1, 3.1.2, and 3.1.3 until we obtain convergence. The culmination of all of these procedures is given in algorithm 2.

Algorithm 2 Boson star evolution code given initial data $\boldsymbol{Y}^0$

```
1: procedure EVOLVE(Y^0)
2:     for j  1, N do                                  ▷ Evolve data for N time steps
3:         Y^j  Y^j 1                ▷ Use data at time j  1 as our guess for data at time j
4:         while Y^j hasn't converged do
5:             UPDATEXI(Y^j)          ▷ Updates for hyperbolic equations, details in 3.1.1
6:             UPDATEPI(Y^j)
7:
8:             UPDATEALPHA(Y^j)          ▷ Updates for elliptic equations, details in 3.1.2
9:             UPDATEBETA(Y^j)
10:            UPDATEPSI(Y^j)
11:
12:            UPDATEPHI(Y^j)                ▷ Updates for scalar elds, details in 3.1.3
13:        end while
14:    end for
15:    return Y^N
16: end procedure
```

Note that each of the update functions does only *one pass* of the corresponding iteration. That is, in the update function for the hyperbolic equations we perform the update (3.30) once for each k = 1, 2, 3 and i = 0, 1, 2, ..., N 1. In the update function for the elliptic equations, we perform one iteration of Gauss-Newton-Seidel relaxation. However, we keep running updates on the data $\boldsymbol{Y}^j$ until the amount by which $\boldsymbol{Y}^j$ changes is below a certain threshold.

Also note that the initial data $\boldsymbol{Y}^0$ is overconstrained. We only need to specify the initial eld values $_1$, $_2$, $_3$ and their time derivatives $_{-1}$, $_{-2}$, $_{-3}$ at t = 0, since the variables ξ_1, ξ_2, ξ_3, $_1$, $_2$, $_3$ can be recovered from their de nitions (3.8) and the initial metric functions α, β, ψ are xed by the elliptic constraints (3.18), (3.16), and (3.14) respectively. Therefore, one can compute the correct initial data $\boldsymbol{Y}^0$ for given $_1$, $_2$, $_3$, $_{-1}$, $_{-2}$, $_{-3}$ by rst assigning the variables ξ_1, ξ_2, ξ_3, $_1$, $_2$, $_3$ as de ned, initializing α, β, ψ to Minkowski space, and then repeatedly performing Gauss-Newton-Seidel iteration as detailed in section 3.1.2. A schema of this procedure is given in algorithm 3.

For our numerical computations, the initial data will correspond to a boson star from chapter 2 for the complex scalar eld $_C$ and a small incoming perturbation for the real

Algorithm 3 Computing initial data $\boldsymbol{Y}^0$ for given $_k, -_k$

procedure COMPUTEINITIALDATA($_1, \ _2, ..., -_1, -_2, ...$)
  (α, β, ψ) MINKOWSKIMETRIC
  $(\xi_1, \xi_2, ..., \ _1, \ _2, ...)$ COMPUTEFIELDDERIVATIVES($_1, \ _2, ..., -_1, -_2, ...$)
  while α, β, ψ haven't converged **do**
    UPDATEALPHA(α) ▷ Updates for elliptic equations, details in 3.1.2
    UPDATEBETA(β)
    UPDATEPSI(ψ)

    UPDATEPI($_1, ..., \ _k$) ▷ Update the xi using the de nitions (3.8)
  end while
  $\boldsymbol{Y}^0$ ($_1, \ _2, ..., \xi_1, \xi_2, ..., \ _1, \ _2, ..., \alpha, \beta, \psi$)
  return $\boldsymbol{Y}^0$
end procedure

scalar eld $_R$ as was done in the simulations by Choptuik and Hawley described in section 1.3.2.

As a nal note on this algorithm, using Bircho 's Theorem, we can de ne a mass aspect function $M(r,t)$ which will equal the total mass of the spacetime when r is large enough such that all the mass of the spacetime is contained inside the sphere of radius r centered at the origin. $M(r,t)$ has the form

$$M(r,t) = \frac{r\psi^6}{18\alpha^2}(r\beta^{\prime} \quad \beta)^2 \quad 2r^2\psi^{\prime}(r\psi)^{\prime}. \tag{3.42}$$

This expression is useful for debugging purposes, as it should be equal to zero at the origin and be monotonically increasing as r grows larger. Another useful tactic for debugging, discussed at greater length in the upcoming section, is to check residuals for equations which are not explicitly used in the evolution code. For example, we would expect the residual for the maximum slicing condition (3.9) to converge to zero as we increase the grid resolution. If it doesn't, we an indication that something is incorrect.

3.1.5 Notes on Convergence

We take this section to brie y discuss some aspects of the convergence of a nite di erence approximation to the continuum solution of a partial di erential equation. Usually when discussing this topic, one takes the approach of viewing the nite di erence approximation

in the continuum regime, as the combination of the true continuum solution and an error which comes from discretization. First and foremost, consider for example, a continuum PDE given by

$$Lu = f, \tag{3.43}$$

where L is some differential operator. Suppose we have some finite difference version of L given by L^h, where h denotes the grid size. The corresponding finite difference approximation with explicit dependence on h is written as

$$L^h u^h = f^h. \tag{3.44}$$

The *truncation error* of the approximation is then given by

$$\tau^h \quad L^h u \quad f^h. \tag{3.45}$$

Naturally, the first goal of any finite difference approximation is to have a scheme for which u^h converges to the true solution u when $h \to 0$. But on top of this baseline concern, one also must consider the rate at which the convergence $u^h \to u$ happens. A finite difference approximation is said to be *p-th order accurate* if it satisfies

$$\tau^h = O(h^p), \tag{3.46}$$

as $h \to 0$. Typically, a finite difference scheme will only be as accurate as the least accurate finite difference operator used in L^h.

In practice, measuring the order of a finite difference scheme is done by a series of a successive mesh refinements. In analogy to a Taylor expansion around the continuum solution u, one assumes a Richardson ansatz for the finite difference approximation u^h,

$$u^h(x,t) = u(x,t) + h\epsilon_1(x,t) + h^2\epsilon_2(x,t) + h^3\epsilon_3(x,t) + \dots, \tag{3.47}$$

where $\epsilon_n(x,t)$ are continuum error functions which do not depend on the value of the grid parameter h.

Clearly, if one has second order accuracy, one expects the ϵ_1 term in the above Richardson expansion to be zero. The same is true for ϵ_2 and third order accuracy. Therefore, it is

possible to con rm the accuracy of a numerical scheme by comparing u^h at di erent grid resolutions, where the grids are re nements of each other. One can de ne the *convergence factor* $Q_h(t)$ as

$$Q_h(t) \quad \frac{\|u^{4h} \quad u^{2h}\|_2}{\|u^{2h} \quad u^h\|_2}, \tag{3.48}$$

where $\|u\|_2$ denotes the L2 norm over the spatial component of u as a function of t. Substitution of the Richardson expansion into the above equation results in

$$Q_h(t) = \frac{\|2h\epsilon_1 + 12h^2\epsilon_2 + O(h^3)\|_2}{\|h\epsilon_1 + 3h^2\epsilon_2 + O(h^3)\|_2}. \tag{3.49}$$

Hence, for rst order accurate schemes, we expect $Q_h(t) \; ! \; 2$ as $h \; ! \; 0$, and likewise for second order accurate schemes, where $\epsilon_1 = 0$, we expect $Q_h(t) \; ! \; 4$ as $h \; ! \; 0$, and so on for higher order schemes.

Measurement of the convergence factor $Q_h(t)$ allows one to determine if a nite di erence scheme is converging, as well as the rate of convergence. However, a priori, it isn't necessarily clear that a nite di erence approximation u^h should converge to a valid continuum solution u as $h \; ! \; 0$. Fortunately, we have the following theorem by Peter Lax,

Theorem 1 (Lax) *If a di erence operator $L^h u^h = f^h$ approximates a di erential operator $Lu = f$ and the resulting nite di erence scheme is stable, then the solution u^h converges to u.*

Thus, as long as our numerical scheme is stable, and measurements of the convergence factor $Q(h)$ coincide with expectations, we can be reasonably con dent that the result u^h does indeed approximate the continuum solution u to the equation $Lu = f$, where L is the di erential operator which L^h approximates.

On the other hand, there is also the question of whether L^h is in fact approximating the correct di erential operator L. One could imagine a situation where the operator L^h is implemented incorrectly due to human error, but the result u^h still converges to the continuum solution of a di erent di erential equation. To factor out this scenario, one can consider alternate forms of the desired equations. In our case, the hyperbolic maximal slicing eq. (3.9) plays precisely this role. If the operator L^h correctly approximates L, then

one expects the residual of (3.9) to converge to zero at the appropriate rate. It would be almost inconceivable that a human error in the implementation of the operator L^h would lead to a scheme for which the residual of (3.9) converges to zero. Therefore, we will use the convergence of (3.9) to zero to verify the correctness of our numerical scheme in the results section.

3.2 Results and Observations

By the end of this project, we were successfully able to implement the numerical relativity code outlined in the previous section. The development of the code took place during the course of the second half of the semester, and our first results were produced close to the end of the project { roughly a week and a half before its conclusion. Thus, while we were able to produce a working second order code for simulating the perturbation of boson stars, there are still a large number of avenues for future work.

Nonetheless, this section will give an overview of what we did manage to accomplish in the time span allotted for this project. Once again, this section uses natural units ~ = c = G = 1 as described in section 2.2.3. We first verify the correctness of the code we produced using the criteria set forth in section 3.1.5. We give the appropriate evidence that the code does indeed converge in second order to the continuum solution. Afterwards, we'll take a brief look at dynamical simulations of slightly-perturbed mini-boson stars from chapter 2, which we managed to produce using our code. We'll also brie y describe future work in the remaining section.

3.2.1 Verification of Second Order Convergence

As explained in section 3.1.5, perhaps the most powerful test of convergence and correctness is to examine the residual of the maximal slicing condition (3.9) and see if it converges to zero at the appropriate rate. The Crank-Nicolson nite di erence form of the maximal

slicing condition (3.9) can be written as

$$R^j \quad r_t\psi \quad \frac{1}{2}L[\boldsymbol{Y}^j] \quad \frac{1}{2}L[\boldsymbol{Y}^{j\ 1}], \tag{3.50}$$

where the nite di erence operator L is given by

$$L[\boldsymbol{Y}] \quad \beta\left(\frac{\psi}{3r} + \delta_r[\psi]\right) + \frac{\psi\,\delta_r[\beta]}{6}. \tag{3.51}$$

To verify that nite di erence code we have implemented is second order accurate and converges to the correct continuum solution, we need to verify empirically that

$$R^{(h)} \ ! \ 0, \qquad Q(t) \ ! \ 4, \tag{3.52}$$

as $h \ ! \ 0$, where $R^{(h)}$ denotes the residual at grid spacing h. To do this, we use a set of initial data in which all of the elds $_k$ interact with each other, evolve the data with the code and then use the result to check (3.52). We take both $_1$ and $_2$ to be Gaussian at the origin, and we let $_3$ be an incoming Gaussian packet from some su ciently far away distance. After a period of time, the incoming packet $_3$ makes contact with $_1$ and $_2$ and there is interference through the gravitational eld. Afterwards, $_3$ re ects o the origin and eventually disappears when it is far enough away due to Sommer eld radiation conditions. The initial data is given by

$$\begin{aligned}
&_1(r,0) = A_1\exp(\ r^2/2\sigma_1^2), && _1(r,0) = 0,\\
&_2(r,0) = 0, && _2(r,0) = A_1\exp(\ r^2/2\sigma_1^2),\\
&_3(r,0) = A_2\exp(\ (r\ \ r_2)^2/2\sigma_2^2), && _3(r,0) = \ \ _3(r,0).
\end{aligned} \tag{3.53}$$

We then set $\xi_k(r,0) = \ ^0_k(r,0)$ and initialize α,β,ψ via the iterative relaxation procedure described in algorithm 3, excluding the updates of $_k$. One must take care to choose A_1, A_2, σ_1, and σ_2 small enough such that the result does not form a singularity. We use the values

$$\begin{aligned}
&r_2 = 60, && A_1 = 0.01, && \sigma_1 = 12,\\
&m = 0.2, && A_2 = 0.006, && \sigma_2 = 8,
\end{aligned} \tag{3.54}$$

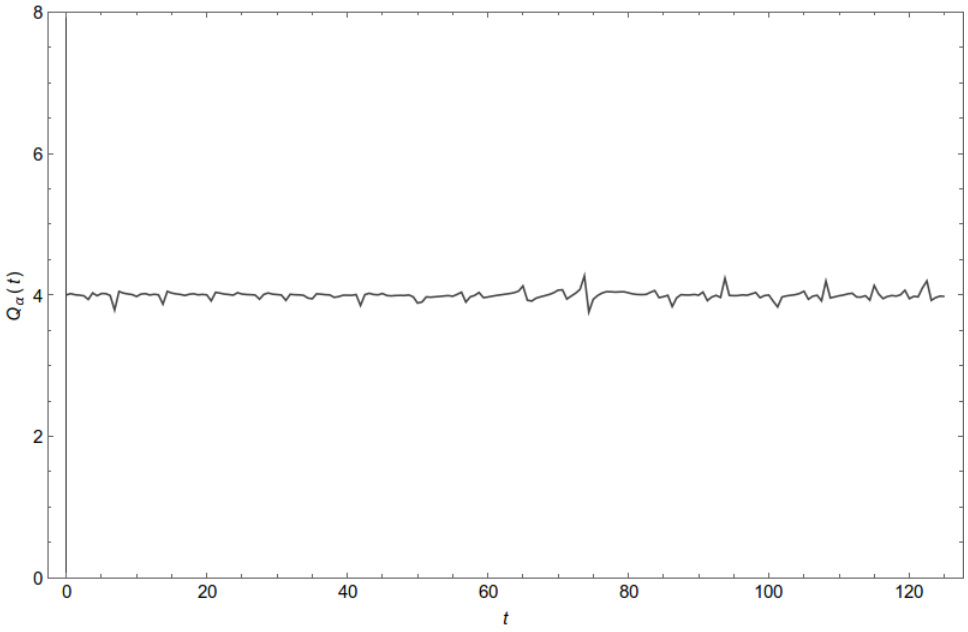

Figure 3.1: Convergence factor $Q_\alpha(t)$ for α

and perform the simulation on the region $[0, B]$, where B = 160. The time step is set to

$$t = h/2\,. \tag{3.55}$$

We run the simulation for a total time of T = 125. This provides enough time for the incoming pulse $_3$ to perturb the boson star at the origin and re ect back.

Our results for convergence are as follows. Using grid sizes N = 1025, N = 2049, and N = 4097, we compute convergence factors for the metric variables α, β, and ψ, as well as the variable $_1$ shown in gures 3.1, 3.3, 3.2, and 3.4, respectively.

As we can see, the convergence factor is approximately four, as expected for a second order accurate numerical scheme. Thus, we are quite con dent in saying that our numerical scheme is second order accurate.

Now, the fact that $Q(t)$! 4 for the eld variables tells us that the scheme converges, but it still remains to be shown that it converges to the correct solution. We do this by examining the residual $R^{(h)}$. Since $R^{(h)}$! 0 in the continuum, we measure the modi ed convergence factor

$$\tilde{Q}_R(t) \quad \frac{kR^{(2h)}k_2}{kR^{(h)}k_2}\,. \tag{3.56}$$

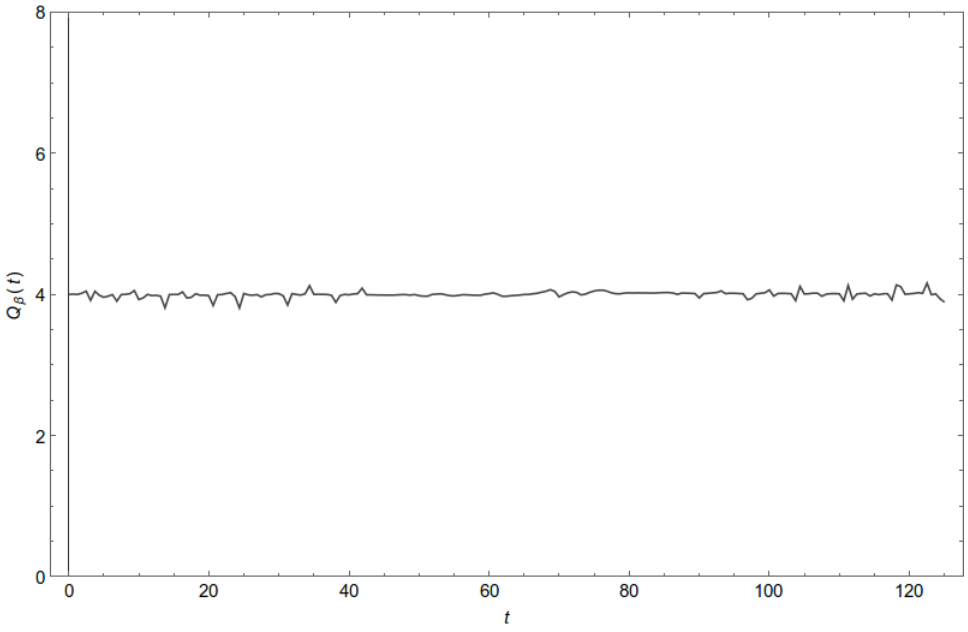

Figure 3.2: Convergence factor $Q_\beta(t)$ for β

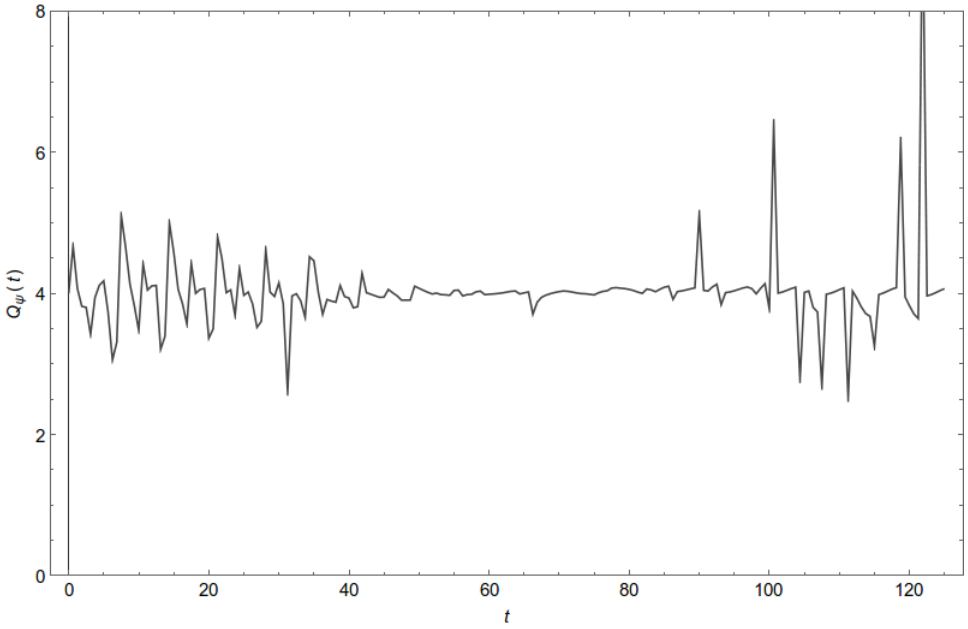

Figure 3.3: Convergence factor $Q_\psi(t)$ for ψ

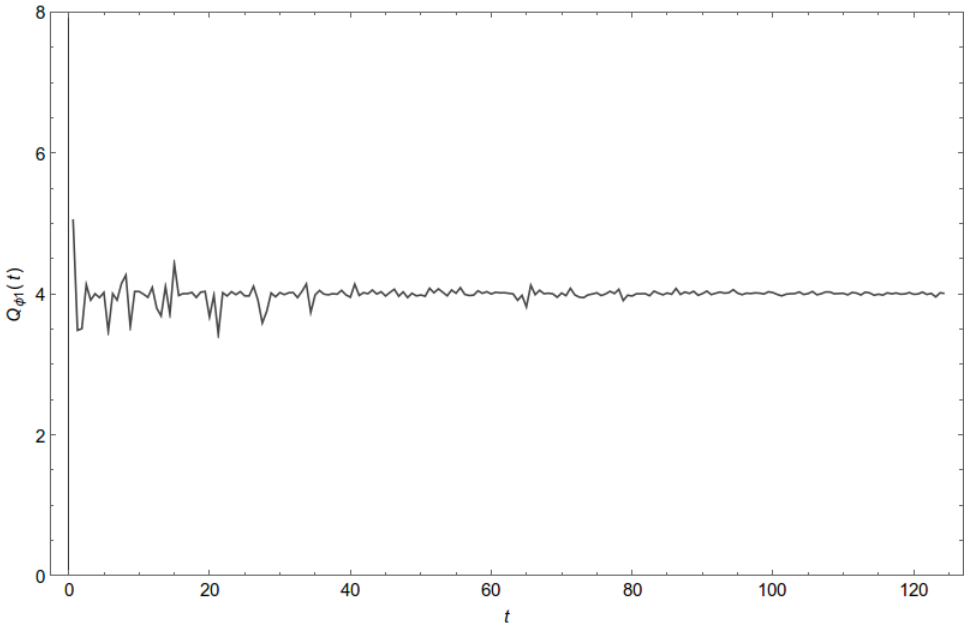

Figure 3.4: Convergence factor $Q_{\ 1}(t)$ for $_1$

Since the continuum solution is 0, the Richardson expansion tells us that we should have $\bar{Q}_h(t) \to 4$. Unfortunately, the convergence factor for $\bar{Q}_h(t)$, shown in figure 3.5 is much more erratic than those we have seen for the variables α, β, ψ, and $_1$. This erratic behavior is due in part to the very fast oscillation of the residual. We use the convergence factor $Q(t)$ instead of $Q(t)$, because this fast oscillation, coupled with the fact that the difference between residuals on successive resolutions is often very close to zero, makes it difficult to see sensible patterns at reasonable resolutions. Although fourth order convergence is hard to see at this resolution, we note that there is convergence, as the factor is consistently above 1. Moreover, note that the scale of the residual is very small in comparison to the scale of the system, as seen in figure 3.6. From our experiments, the residual remains at this scale throughout the evolution. This is also true for lower resolutions. As per the discussion of convergence in section 3.1.5, all these considerations lead us to believe that the system converges to the correct solution as $h \to 0$.

However, there is a slight caveat involved in the convergence of the residual. Since we are performing calculations on a bounded domain $[0, B]$, the boundary conditions at $r = B$

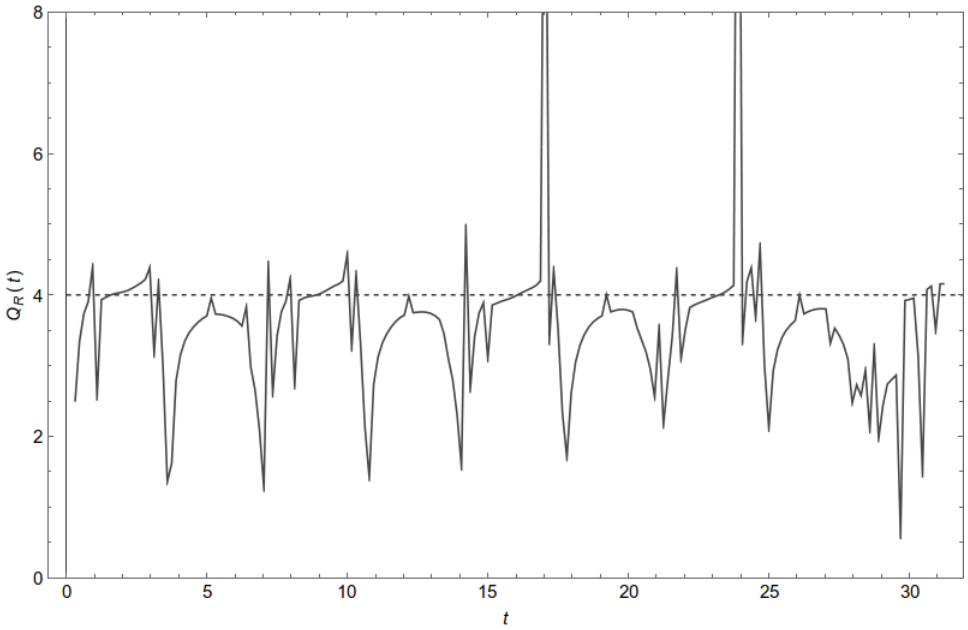

Figure 3.5: Convergence factor $\tilde{Q}_R(t) = kR_{2h}k_2/kR_hk_2$ for the residual R of the maximal slicing condition. Measured with grid sizes N = 2049 and N = 4097 with B = 640. At spikes where the the factor drops below 2, R_{2h} and R_h become very close to the at false continuum solution induced by the $O(1/r)$ accurate boundary conditions at r = B, hence the convergence factor becomes smaller. Elsewhere, however, the convergence factor falls only slightly below 4.

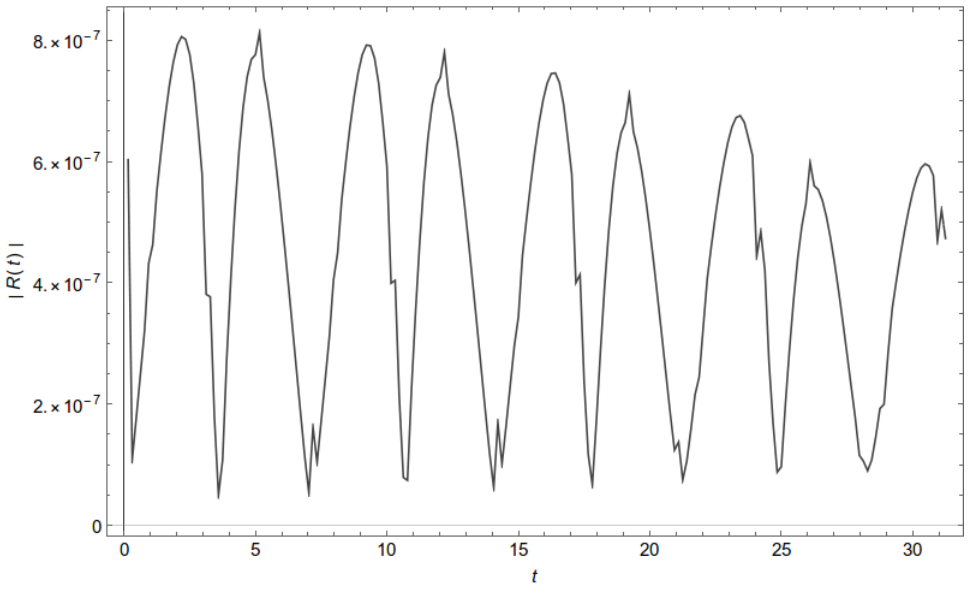

Figure 3.6: Plot of residual L2 norm kRk_2. Measured with grid size N = 2048 with B = 640. Note how the residual is very small in comparison to the scale of the system. For reference, the system operates at scales around 10 ^{2}.

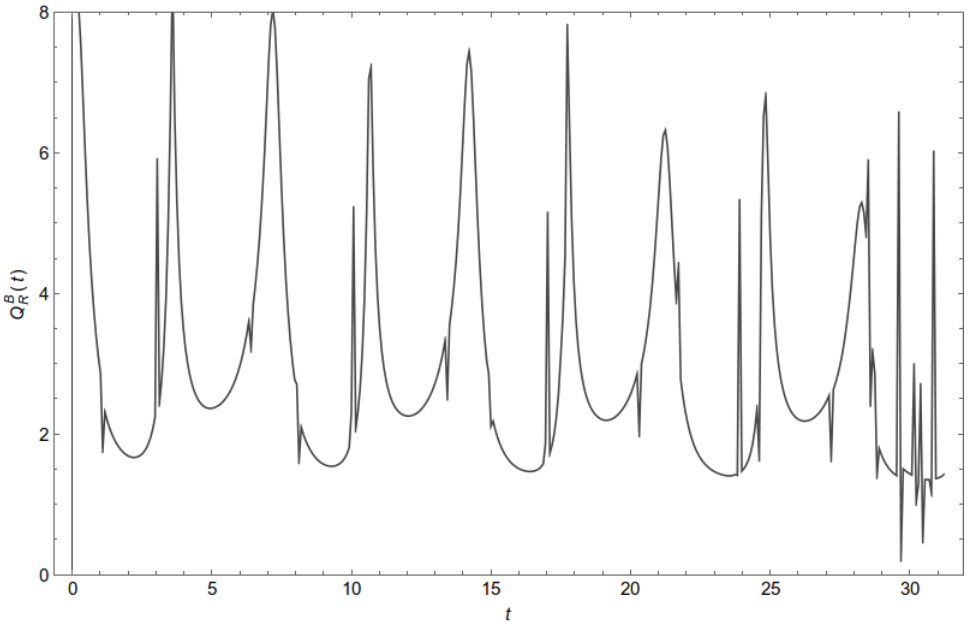

Figure 3.7: Convergence factor $Q_R^B(t) = kR_Bk_2/kR_{2B}k_2$ for the domain size B. Note that the lowest value of the convergence factor is around 2. The domain sizes taken were B = 320 with N = 2049 for the numerator and B = 640 with N = 4097 for the denominator.

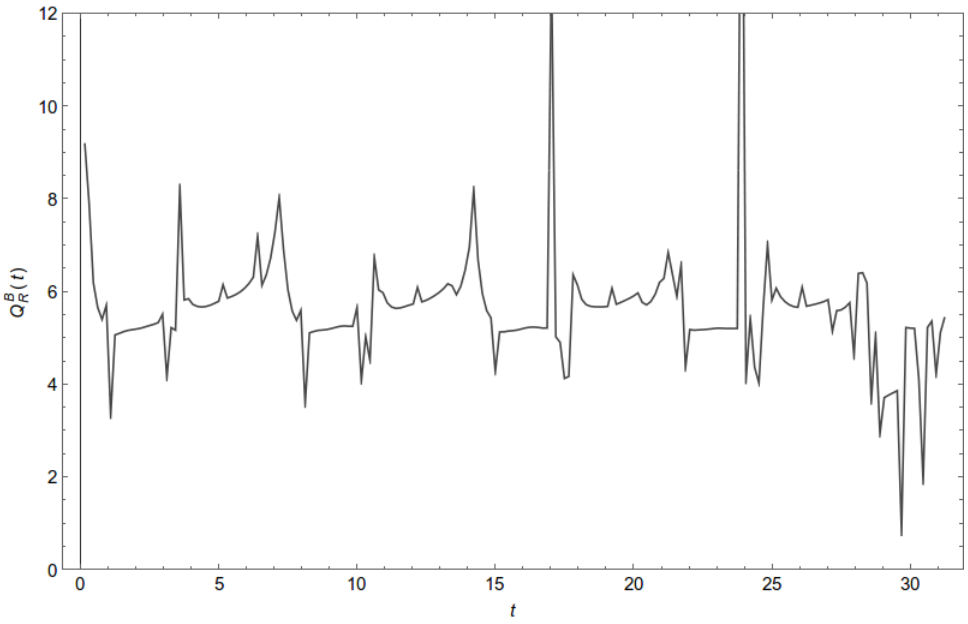

Figure 3.8: Convergence factor $Q_R^B(t) = kR_{2h,B}k_2/kR_{h,2B}k_2$ for the domain size B and grid size N. This convergence factor combines the two in gures 3.5 and 3.7. The domain sizes taken were B = 320 with N = 1025 for the numerator and B = 640 with N = 4097 for the denominator. As we can see, convergence is much clearer in this case, since the factor is consistently above 4.

are only accurate to within $O(1/r)$. Hence, the continuum solution of the numerical scheme is not quite the same as the true continuum solution desired. To counteract this, one takes both the size of the domain $B \to \infty$ as well as the grid spacing $h \to 0$. Only when both of these are done will the result converge to the true solution. One can see in figure 3.5 that increasing the size of the domain does indeed affect the convergence of the residual to zero, as expected. When both the grid spacing and the domain size are increased simultaneously, convergence of R to zero in the numerical scheme becomes much clearer, as seen in figure 3.8.

3.2.2 Case Study: Mini-Boson Stars

As a small case study, we use the numerical code we have developed to look at mini-boson stars from chapter 2. Note that we cannot directly use the output of chapter 2 as initial data for our simulation, since the solver for chapter 2 and the numerical code in this section use different coordinate systems (geodesic slicing vs. maximal slicing). Fortunately, our work in chapter 2 does allow us to compute a corresponding frequency ω for a given central field density $\varphi(0)$. Since the profiles of the mini-boson star ground states are approximately Gaussian with some width we can estimate from results of chapter 2, it is possible to feed approximate initial data into the evolution code of this section and see mini-boson stars with some small perturbation. Indeed, if we have an approximate profile for the field modulus $\varphi(r)$, then we can set initial data to be

$$\begin{aligned} \Psi_1(r,0) &= \varphi(r), & \Psi_{-1}(r,0) &= 0, \\ \Psi_2(r,0) &= 0, & \Psi_{-2}(r,0) &= \omega\varphi(r), \end{aligned} \tag{3.57}$$

with $\Psi_3 = \Psi_{-3} = 0$, in the hope that we will find a solution close to the desired solution $\Psi_C = \varphi e^{i\omega t}$.

As an example, we use the central field density $\varphi(0) = 0.05$ and corresponding ω from our computation in table 2.1, our guess for $\varphi(r)$ is a Gaussian with corresponding amplitude and $\sigma = 3.285$. The numerical code does produce an observable boson star oscillating as expected between the real component Ψ_1 and the complex component Ψ_2 of the boson star's

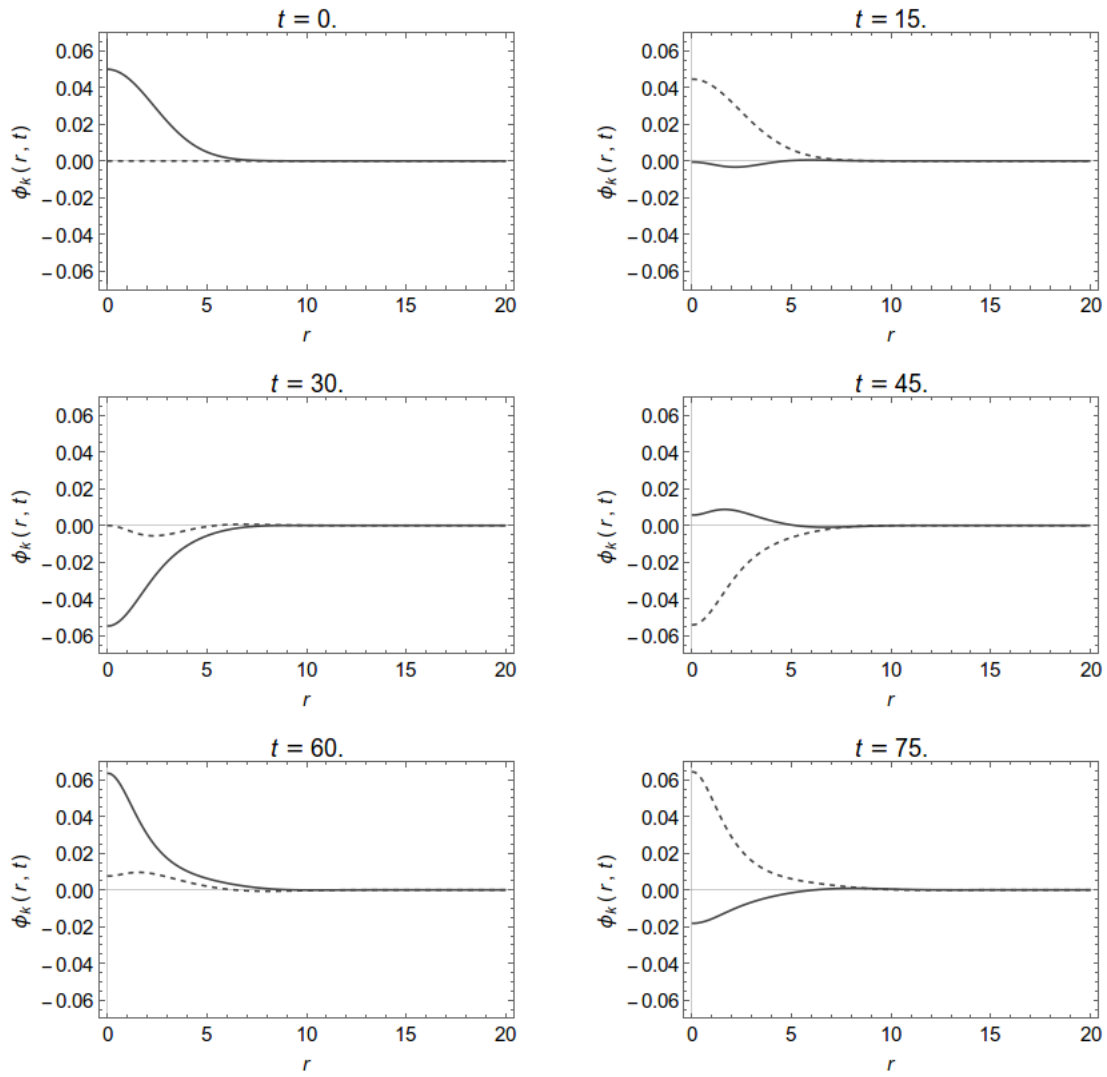

Figure 3.9: Plots of the real and imaginary component of the complex scalar eld $_C$ at six di erent times. The real component $_1$ is depicted by the solid line, while the imaginary component $_2$ is depicted by the dashed line. Note that the two components approximately rotate into each other as time passes, as expected for a mini-boson star $_C(r,t) = \varphi(r)e^{i\omega t}$ plus some perturbation.

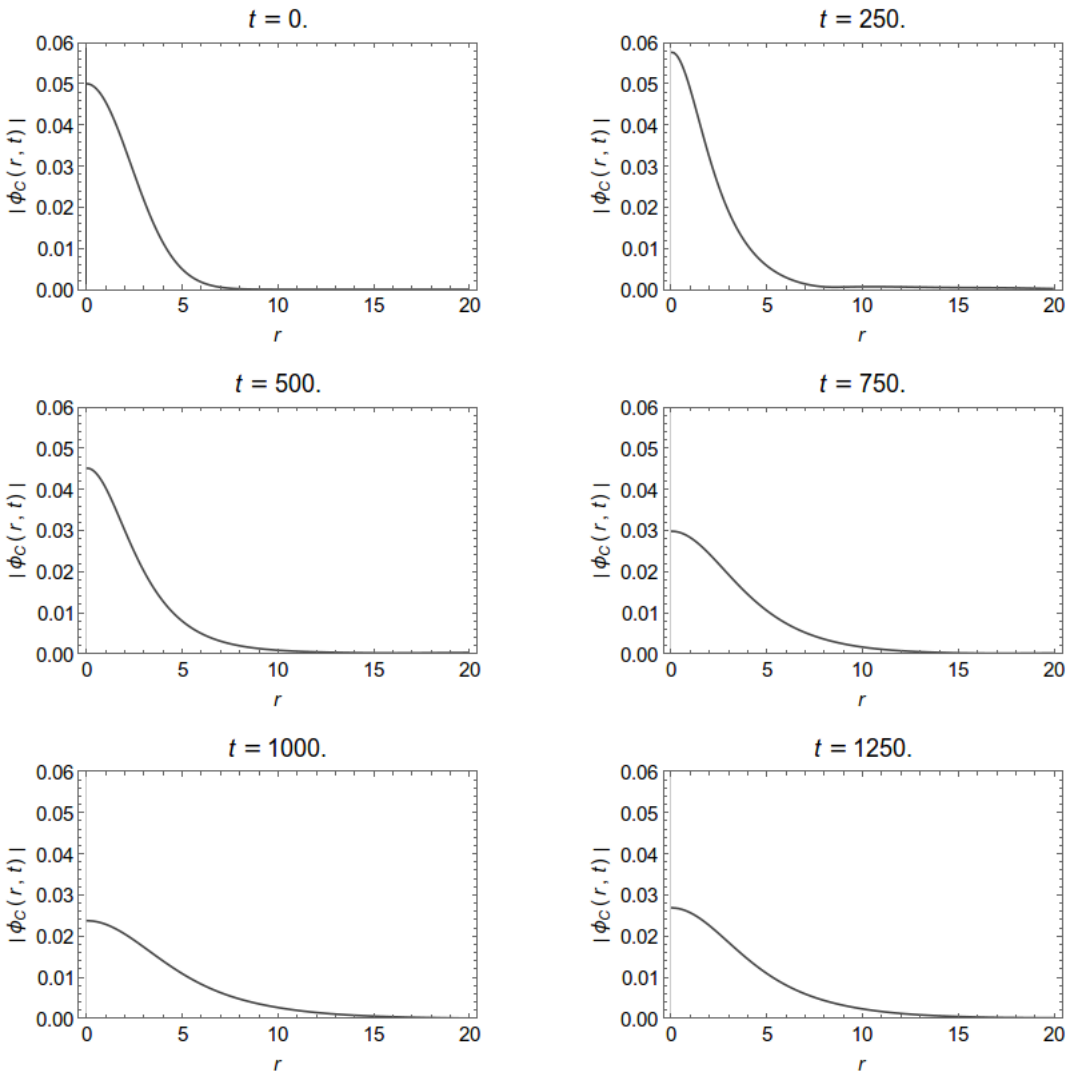

Figure 3.10: Plots of the modulus $|\phi_C|$ of the complex scalar field at different times. The time scale shown is significantly larger than that of figure 3.9. While the profile always remains approximately Gaussian, there is a definite change in the density and radius of the star over a long period time. This is a part of an oscillating cycle of decay and excitation which takes place over a larger time scale.

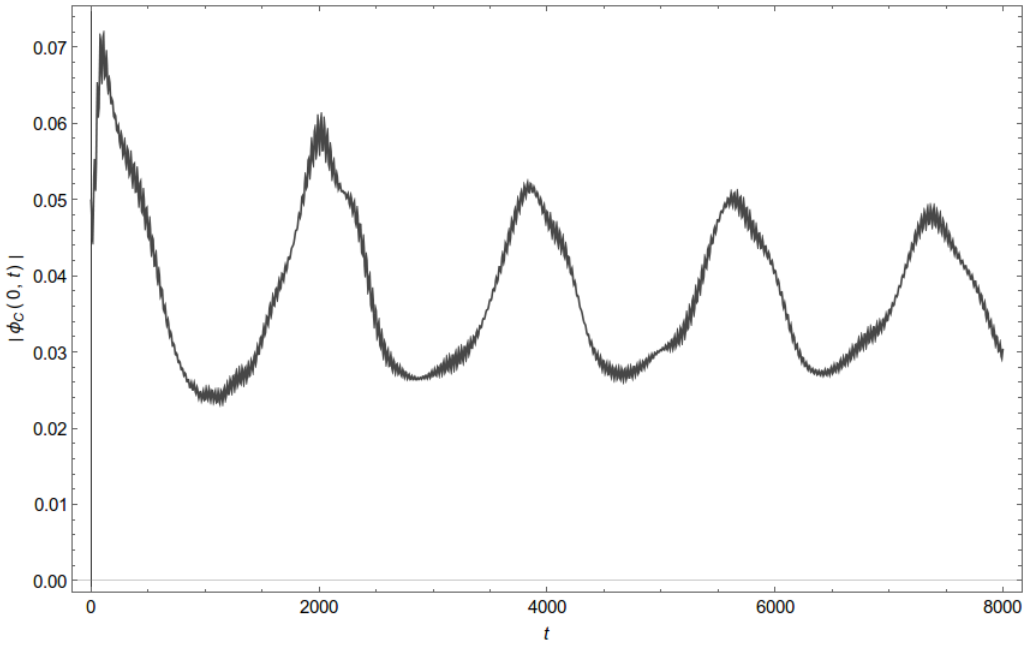

Figure 3.11: Central eld density $j_C(0,t)j$ as a function of time over a large time scale. Note the oscillation of the central density over time, this parallels the behavior seen in gure 3.10.

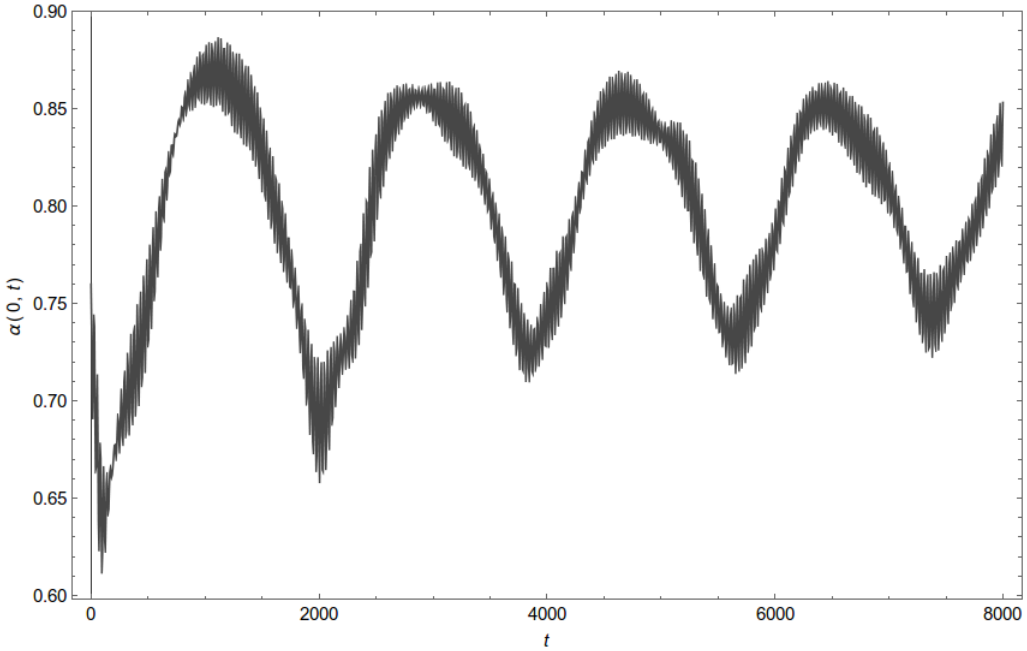

Figure 3.12: Central value of the lapse function $\alpha(0,t)$ as a function of over a large time scale. Note the oscillation over time.

complex scalar field. The initial results of this computation can be seen in figure 3.9. We achieve something approximately like a complex scalar field with a rotating phase – we can clearly see that the Gaussian-like profile rotates from $_1$ into $_2$ and then back, with a slight added perturbation. As desired, this rotating behavior seems to persist indefinitely. However, after an initial period where the star radiates some scalar matter to infinity, there is a very gradual change in the profile of the star as can be seen in figure 3.10. We computed all the results in this section on a grid of $N = 257$ spatial samples and domain size $B = 20$.

Although the rotating behavior persists and the modulus $j_C j$ of the complex scalar field looks relatively constant over a short period of time, over larger time scales the profile of the star goes through periodic cycles of decay and excitation – the radius and density of the star oscillates periodically over a long time period which seems to continue perpetually. This oscillation can be seen in figure 3.11, which shows the modulus central field density over a long period of time. It can also be seen in the central value of the lapse function α, shown in figure 3.12. We believe that this behavior is due to beating among the modes of the initial perturbation.

3.2.3 Future Work

So far we have evolved approximate ground states of mini-boson stars with the numerical code developed during the course of this project. The next step in this project is to use above numerical code to perturb a thin-wall ground state of a solitonic boson star. Unfortunately, solitonic boson stars are more sensitive to initial conditions than the mini-boson stars we evolved in section 3.2.2. Therefore, we can neither estimate the profile of a thin-wall ground state like we did for mini-boson stars in section 3.2.2 nor use the profile computed in chapter 2 directly, because the evolution code in this chapter uses a different coordinate system than the coordinate system we use in chapter 2. However, a computation for stationary states with the rotating phase ansatz $_C(r,t) = \varphi(r)e^{i\omega t}$ analogous to the computation done in section 2.1 can be done in this new maximal slicing gauge. An explicit substitution of the ansatz into the governing eqs. (3.10), (3.14), (3.16), and (3.18), and dropping the time

dependence of the metric variables α, β, and ψ provides the following equations:

$$\frac{d^2\varphi}{dr^2} = \frac{1}{r\alpha\psi(\alpha^2 \quad \beta^2\psi^4)}\Big[\quad r\omega^2\alpha\varphi\psi^5 + r\alpha^3\varphi\psi^5\frac{dV}{d\varphi^2} \quad 2\alpha^3\psi\varphi' + 2\alpha\beta^2\psi^5\varphi' \quad r\alpha^2\psi\alpha'\varphi'$$
$$r\beta^2\psi^5\alpha'\varphi' + 2r\alpha\beta\psi^5\beta'\varphi' \quad 2r\alpha^3\varphi'\psi' + 6r\alpha\beta^2\psi^4\varphi'\psi'\Big],$$
$$\frac{d^2\alpha}{dr^2} = \frac{1}{3r^2\alpha\psi}\big[\quad 3r^2\kappa V(\varphi^2)\alpha^2\psi^5 + 2\beta^2\psi^5 + 6r^2\kappa\omega^2\varphi^2\psi^5 \quad 6r\alpha\psi\alpha'$$
$$r\beta^2\psi^5\alpha'\varphi' + 2r\alpha\beta\psi^5\beta'\varphi' \quad 2r\alpha^3\varphi'\psi' + 6r\alpha\beta^2\psi^4\varphi'\psi'\big],$$
$$\frac{d^2\beta}{dr^2} = \frac{1}{r^2\alpha\psi}\big[\quad 3r^2\kappa V(\varphi^2)\alpha^2\psi^5 + 2\beta^2\psi^5 + 6r^2\kappa\omega^2\varphi^2\psi^5 \quad 6r\alpha\psi\alpha'$$
$$4r\beta\psi^5\beta' + 2r^2\psi^5(\beta')^2 + 6r^2\kappa\beta^2\psi^5(\varphi')^2 \quad 6r^2\alpha\alpha'\psi'\big],$$
$$\frac{d^2\psi}{dr^2} = \frac{1}{12r^2\alpha^2}\big[3r^2\kappa V(\varphi^2)\alpha^2\psi^5 + \beta^2\psi^5 + 3r^2\kappa\omega^2\varphi^2\psi^5 \quad 2r\beta\psi^5\beta'$$
$$r^2\psi^5(\beta')^2 + 3r^2\kappa\alpha^2\psi(\varphi')^2 + 3r^2\kappa\beta^2\psi^5(\varphi')^2 + 24r\alpha^2\psi'\big].$$

(3.58)

As we can see, these equations are second order in the metric variables α, β, ψ. Moreover, since we have the boundary conditions $\alpha(R) = 1$, $\beta(R) = 0$, $\psi(R) = 1$, implementing a solver for this ODE system will require a nontrivial extension to the work in chapter 2, a very clear direction for future work on this project. The next obvious step is to implement a solver for the system (3.58), nd the desired thin-wall ground states, and use the result as initial data for the code implemented in this chapter, using an appropriate perturbation.

Appendix A

The 3+1 Decomposition and ADM Formalism

A.1 Foliations of Spacetime

A signi cant drawback to the standard tensorial formulation (1.1) of the Einstein equations is that it treats time and space on equal footing. Unfortunately, while this formulation does have its perks, our goal is to study the evolution of some form of initial data on a cross-section of the Pseudo-Riemannian manifold ($M, g_{\mu\nu}$). This is typically done in the context of a foliation of the spacetime into space like slices. In this framework, we suppose that M can be foliated into spacelike slices $_t$ parametrized by some global time function t. The derivative of t gives us a timelike 1-form,

$$_\mu \quad r_\mu t . \tag{A.1}$$

We'll de ne the *lapse function* α using the norm of under the metric $g_{\mu\nu}$,

$$\frac{1}{\alpha^2} \quad g^{\mu\nu} \ _\mu \ _\nu . \tag{A.2}$$

[0] This appendix is a modi ed excerpt taken with permission from a paper submitted for MAT522: Introduction to PDE

Take ω_μ α $_\mu$ to be the 1-form $_\mu$ normalized to length 1. The unit normal to the slices $_t$ can now be de ned as the reoriented dual of this normalized 1-form,

$$n^\mu \quad \omega^\mu , \tag{A.3}$$

where the negative sign is to ensure that n^μ points in the direction of increasing t,

$$n^\mu \omega_\mu = \quad g^{\mu\nu}\omega_\mu\omega_\nu = 1 . \tag{A.4}$$

Furthermore, the normal n^μ is constructed so that $n^\mu n_\mu =$ 1, hence n^μ is timelike.

The normal vector n^μ allows us to the de ne the projection operator onto n^μ as well as the projection operator onto the orthogonal complement of n^μ, respectively given by

$$P^\mu{}_\nu \quad n^\mu n_\nu \qquad \gamma^\mu{}_\nu \quad \delta^\mu{}_\nu + P^\mu{}_\nu . \tag{A.5}$$

To nd a Riemannian metric for the individual slices $_t$, we want to project out everything which lies along the vector n^μ. This will allow us to de ne a purely spatial metric tensor for $_t$. Therefore, we'll take the metric tensor $g_{\mu\nu}$ and project both indices using the operator $\gamma^\mu{}_\nu$. This gives

$$g_{\alpha\beta}\gamma^\alpha{}_\mu\gamma^\beta{}_\nu = g_{\alpha\beta}(\delta^\alpha{}_\mu + n^\alpha n_\mu)(\delta^\beta{}_\nu + n^\beta n_\nu) = g_{\mu\nu} + 2n_\mu n_\nu + g_{\alpha\beta}n^\alpha n^\beta n_\mu n_\nu = g_{\mu\nu} + n_\mu n_\nu . \tag{A.6}$$

We note that this is in fact:

$$g_{\alpha\beta}\gamma^\alpha{}_\mu\gamma^\beta{}_\nu = g_{\mu\nu} + n_\mu n_\nu = \gamma_{\mu\nu} . \tag{A.7}$$

Therefore $\gamma_{\mu\nu}$ is a purely spatial metric on the time slices $_t$. To de ne a covariant derivative compatible with the spatial metric $\gamma_{\alpha\beta}$, one may take a covariant derivative on *M* and project the result with the projection tensor $\gamma^\mu{}_\nu$. Therefore, the spatial covariant derivative corresponding to the metric $\gamma_{\alpha\beta}$ for a spatial (n, m)-tensor is given by

$$D_\mu T^{\alpha_1\alpha_2\ldots\alpha_n}{}_{\beta_1\beta_2\ldots\beta_m} \quad \gamma^{\alpha_1}{}_{\alpha'_1}\gamma^{\alpha_2}{}_{\alpha'_2}\ldots\gamma^{\alpha_n}{}_{\alpha'_n}\gamma^{\beta'_1}{}_{\beta_1}\gamma^{\beta'_2}{}_{\beta_2}\ldots\gamma^{\beta'_m}{}_{\beta_m}\gamma^{\mu'}{}_\mu \, r_{\mu'} T^{\alpha'_1\alpha'_2\ldots\alpha'_n}{}_{\beta'_1\beta'_2\ldots\beta'_m} . \tag{A.8}$$

One can verify that this derivative satis es all the requisite properties of a covariant derivative compatible with the metric $\gamma_{\mu\nu}$.

This covariant derivative for spatial tensors has its own connection coe cients, given by

$$^{(3)}\ \sigma_{\mu\nu} = \frac{1}{2}\gamma^{\sigma\rho}(\partial_\nu\gamma_{\rho\mu} + \partial_\mu\gamma_{\rho\nu} \quad \partial_\rho\gamma_{\mu\nu}) . \tag{A.9}$$

As well as its own Riemann tensor, given by

$$^{(3)}R^{\sigma}{}_{\alpha\beta\rho} = \partial_\beta{}^{(3)}\ \sigma_{\rho\alpha} + \partial_\rho{}^{(3)}\ \sigma_{\beta\alpha} + {}^{(3)}\ \sigma_{\beta\lambda}{}^{(3)}\ \lambda_{\rho\alpha} \quad {}^{(3)}\ \sigma_{\rho\lambda}{}^{(3)}\ \lambda_{\beta\alpha} . \tag{A.10}$$

This tensor measures the *internal* curvature of the surface $_t$. However, it carries no information about the shape the $_t$ takes relative to the ambient geometry of *M*.

A.2 The Second Fundamental Form

In classical di erential geometry, the **second fundamental form** of a smooth surface *M* is de ned as

$$\text{II} \qquad d\vec{N}\ \ d\vec{x} . \tag{A.11}$$

That is, the second fundamental form measures the change of the normal vector $\vec{N}$ of the surface in a speci c direction $d\vec{x}$ in the tangent space TM. In the framework of foliations of spacetime, this corresponds precisely to taking the covariant derivative of the normal vector n^μ. Therefore, it is natural to de ne the second fundamental form of $_t$ as

$$K_{\mu\nu} \qquad D_\mu n_\nu = \quad \gamma^\alpha{}_\mu\gamma^\beta{}_\nu\, r_\alpha n_\beta . \tag{A.12}$$

One can verify that $K_{\mu\nu}$ is actually symmetric due to the properties of n^μ,

$$K_{[\mu\nu]} = 0 . \tag{A.13}$$

Alternatively, we can express $K_{\mu\nu}$ as the Lie derivative of the induced metric $\gamma_{\mu\nu}$,

$$K_{\mu\nu} = \quad \frac{1}{2}L_n\gamma_{\mu\nu} . \tag{A.14}$$

We will not do it here, but one can verify that the de nitions (A.12) and (A.14) are, in fact, equivalent.

The common way to specify initial data for the Einstein equations is to use both the induced spatial metric $\gamma_{\mu\nu}$ and the second fundamental form $K_{\mu\nu}$, sometimes called the **extrinsic curvature tensor**, as initial data. However, we must take care when doing this. Just as in classical di erential geometry, there are compatibility conditions on the rst fundamental form $\gamma_{\mu\nu}$ and second fundamental form $K_{\mu\nu}$ { not just any initial data is allowed. These compatibility conditions take form of the equations of Gauss, Codazzi, and Ricci, which relate the Riemann tensor $R^{\sigma}{}_{\mu\nu\rho}$ of $g_{\mu\nu}$ to the extrinsic curvature $K_{\mu\nu}$ and the Riemann tensor ${}^{(3)}R^{\sigma}{}_{\mu\nu\rho}$ of the induced metric $\gamma_{\mu\nu}$. These equations can be derived by decomposing the tensor $R^{\sigma}{}_{\mu\nu\rho}$ into spatial and normal components. Expressing the action of the commutator $[D_\mu, D_\nu]$ on a vector eld V^α in terms of a full spatial projection of the Riemann tensor $R_{\sigma\mu\rho\nu}$ and the extrinsic curvature $K_{\mu\nu}$ yields **Gauss' equation**,

$$ {}^{(3)}R_{\sigma\mu\rho\nu} + K_{\sigma\rho}K_{\mu\nu} \quad K_{\sigma\nu}K_{\rho\mu} = \gamma^{\alpha}{}_{\sigma}\gamma^{\beta}{}_{\mu}\gamma^{\delta}{}_{\rho}\gamma^{\epsilon}{}_{\nu}R_{\alpha\beta\delta\epsilon}\,. \tag{A.15} $$

If we were to consider projections of $R^{\sigma}{}_{\mu\rho\nu}$ with one index projected in the normal direction and the remaining three spatially, work out the derivative $D_\sigma K_{\mu\nu}$, and then antisymmetrize, we would arrive at the **Codazzi equation**,

$$ D_\sigma K_{\mu\nu} \quad D_\mu K_{\sigma\nu} = \gamma^{\alpha}{}_{\mu}\gamma^{\beta}{}_{\sigma}\gamma^{\delta}{}_{\nu}n^{\epsilon}R_{\alpha\beta\delta\epsilon}\,. \tag{A.16} $$

Finally, considering projections of $R^{\sigma}{}_{\mu\rho\nu}$ with two indices projected in the normal direction and the remaining two spatially and computing the Lie derivative $L_n K_{\mu\nu}$ would give us **Ricci's equation**,

$$ L_n K_{\mu\nu} = n^{\alpha}n^{\delta}\gamma^{\beta}{}_{\mu}\gamma^{\epsilon}{}_{\nu}R_{\alpha\beta\delta\epsilon} \quad \frac{1}{\alpha}D_\mu D_\nu \alpha \quad K^{\rho}{}_{\mu}K_{\rho\nu}\,, \tag{A.17} $$

where α is de ned in (A.2). For the sake of brevity, we will not provide a derivation of these three equations here. If the reader is inclined, a full derivation of these three equations can be found in section 2.5 of [2].

A.3 The ADM Formulation

The formulations of the previous section are a good start, but now, using our foliation $_t$ of spacetime, we would like to de ne a coordinate system on M which will be useful for producing a 3+1 decomposition of the spacetime. In short, we want to de ne a vector frame $fe_{(0)}, e_{(1)}, e_{(2)}, e_{(3)}g$ and a corresponding coordinate system on M such that $e_{(0)}$ is timelike and $e_{(1)}, e_{(2)}, e_{(3)}$ are purely spatial. The obvious candidate for $e_{(0)}$ would be the normal vector n^a, however, this choice is somewhat unnatural, due to the fact that n^a isn't dual to the 1-form $_a$,

$$_\mu n^\mu = \alpha g^{\mu\nu} r_\mu t r_\nu t = \alpha^{-1}. \tag{A.18}$$

Instead, we use the following connection vector,

$$t^\mu \quad \alpha n^\mu + \beta^\mu, \tag{A.19}$$

where β^μ is a purely spatial vector, that is, $\gamma^\mu{}_\nu \beta^\nu = \beta^\mu$. The vector β^μ is refered to as the **shift vector**. Since $_\mu \beta^\mu = 0$, the vector (A.19) is indeed dual to $_\mu$,

$$_\mu t^\mu = 1. \tag{A.20}$$

The intuitive interpretation of t^μ is that it will connect two points on $_t$ and $_{t+dt}$ with the same spatial coordinates when we are nished constructing our coordinate system. We let our rst frame vector $e_{(0)}$ be t^μ. Now, consider the rst time slice $_0$. The slice $_0$ is diffeomorphic to R^3, hence there exists some natural spatial coordinate system $fx_{(1)}, x_{(2)}, x_{(3)}g$ on $_0$ with a corresponding purely spatial vector frame $fe_{(1)}, e_{(2)}, e_{(3)}g$. But $fe_{(1)}, e_{(2)}, e_{(3)}g$ is only de ned on $_0$ and we want to de ne them everywhere on M. To do this, we may utilize the vector eld t^μ. We can transport the vector frame $fe_{(1)}, e_{(2)}, e_{(3)}g$ onto other time slices by de ning them in terms of a solution to a linear di erential equation, by demanding

$$L_t e^\mu_{(i)} = 0. \tag{A.21}$$

Intuitively, we "drag" the coordinate frame $fe_{(1)}, e_{(2)}, e_{(3)}g$ along the vector eld $e_{(0)} = t^a$. We can easily verify that the the dragged vector elds remain purely spatial,

$$L_t(\ _\mu e^\mu_{(i)}) = L_t\ _\mu e^\mu_{(i)} + \ _\mu L_t e^\mu_{(i)} = 0, \tag{A.22}$$

where $L_{t\ \mu} = 0$ as a result of (A.20). This gives us a vector frame $\mathfrak{B} \quad \{e_{(0)}, e_{(1)}, e_{(2)}, e_{(3)}\}$ on all of M.

The next step is to adopt this vector frame. t^μ now has the coordinate representation

$$t^\mu = \begin{pmatrix} 1 & 0 & 0 & 0 \end{pmatrix}. \tag{A.23}$$

Therefore, the Lie derivative L_t reduces to the partial derivative operator,

$$L_t = \partial_t, \tag{A.24}$$

Furthermore, we note that

$$n_\mu e^\mu_{(i)} = \quad \alpha^{\ 1}\ {}_\mu e^\mu_{(i)} = 0. \tag{A.25}$$

Therefore, since $\{e_{(1)}, e_{(2)}, e_{(3)}\}$ span $T_{\ t}$, we know that in any 3 + 1 coordinate system, the covariant spatial components of n must vanish,

$$n_i = 0. \tag{A.26}$$

Moreover, since all spatial vectors v^μ vanish when contracted with n_μ, we know that $n_0 v^0 = n_\mu v^\mu = 0$ and hence $v^0 = 0$. This means the shift vector β^μ takes the form

$$\beta^\mu = \begin{pmatrix} 0 & \beta^i \end{pmatrix}. \tag{A.27}$$

We may now use the coordinate representations of t^μ and β^μ to solve for the coordinate representation of n^μ using eq. (A.19),

$$n^\mu = \alpha^{\ 1}(t^\mu \quad \beta^\mu) = \begin{pmatrix} \alpha^{\ 1} & \alpha^{\ 1}\beta^i \end{pmatrix}. \tag{A.28}$$

Now, using the fact that n^μ is normalized to -1 and that n_μ has no spatial components, we arrive at

$$n_\mu = \begin{pmatrix} -\alpha & 0 & 0 & 0 \end{pmatrix}. \tag{A.29}$$

With this established, recall that

$$\gamma_{\mu\nu} = g_{\mu\nu} + n_\mu n_\nu. \tag{A.30}$$

Hence, as a direct result of (A.26), the spatial components of γ and g are equal,

$$\gamma_{ij} = g_{ij} \,. \tag{A.31}$$

Moreover, since $\gamma^{\mu\nu}$ is purely spatial contravariant tensor, we also have $\gamma^{\mu 0} = 0$. Using this fact, we can easily write out an expression for the inverse metric $g^{\mu\nu}$ using the relation $g^{\mu\nu} = \gamma^{\mu\nu} \quad n^\mu n^\nu$ and the coordinate expression (A.28),

$$g^{\mu\nu} = \begin{pmatrix} \alpha^{-2} & \alpha^{-2}\beta^i \\ \alpha^{-2}\beta^j & \gamma^{ij} \quad \alpha^{-2}\beta^i\beta^j \end{pmatrix} \,. \tag{A.32}$$

We want to invert this matrix to recover a coordinate form for $g_{\mu\nu}$. This gives us the metric in all its glory,

$$g_{\mu\nu} = \begin{pmatrix} \alpha^2 + \beta_k\beta^k & \beta_i \\ \beta_j & \gamma_{ij} \end{pmatrix} \,, \tag{A.33}$$

where the index of β^i are lowered using the three dimensional tensor γ_{ij}. In alternate notation, this can be written as

$$ds^2 = \quad \alpha^2\, dt^2 + \gamma_{ij}(dx^i + \beta^i\, dt)(dx^j + \beta^j\, dt) \,. \tag{A.34}$$

Conditions on the functions α, β, and γ_{ij} now amount to specifying a gauge. For example, the simplest gauge to specify in the ADM formalism is the geodesic slicing condition, which reads

$$\alpha = 1 \,, \qquad \beta^i = 0 \,. \tag{A.35}$$

In this gauge, normal observers are freely-falling and follow geodesics. However, this gauge cannot handle the formation of trapped surfaces. Thus, a better choice is often to use a *maximal slicing* gauge, in which

$$K^\mu{}_\mu = 0 \,. \tag{A.36}$$

This condition can be written in terms of the decomposed metric variables as

$$D^2\alpha = \alpha(K_{\mu\nu}K^{\mu\nu} + 4\pi(\rho + S)) \,, \tag{A.37}$$

where

$$\rho = n_\mu n_\nu T^{\mu\nu} \qquad S = \gamma^{\mu\nu}S_{\mu\nu} \qquad S_{\alpha\beta} = \gamma_{\alpha\mu}\gamma_{\beta\nu}T^{\mu\nu} \,. \tag{A.38}$$

Appendix B

Source Code

The source code for this project is available online at

`https://github.com/uniqueuptoisomorphism/bosonstars`

This software is provided primarily for archival purposes. In terms of software engineering practice, it does not re ect our best work and is provided without any user or developer documentation.

References

[1] B. Abbott, R. Abbott, T. Abbott, M. Abernathy, F. Acernese, K. Ackley, C. Adams, T. Adams, P. Addesso, R. Adhikari, et al. Properties of the binary black hole merger gw150914. *Physical review letters*, 116(24):241102, 2016.

[2] T. W. Baumgarte and S. L. Shapiro. *Numerical relativity: solving Einstein's equations on the computer*. Cambridge University Press, 2010.

[3] V. Cardoso, S. Hopper, C. F. Macedo, C. Palenzuela, and P. Pani. Gravitational-wave signatures of exotic compact objects and of quantum corrections at the horizon scale. *Physical Review D*, 94(8):084031, 2016.

[4] D.-I. Choi, K. C. Lai, M. W. Choptuik, E. W. Hirschmann, S. L. Liebling, and F. Pretorius. Dynamics of axisymmetric (head-on) mini-boson star collisions. *preprint*, 2010.

[5] M. W. Choptuik. Universality and scaling in gravitational collapse of a massless scalar eld. *Physical Review Letters*, 70(1):9, 1993.

[6] S. Coleman. Q-balls. *Nuclear Physics B*, 262(2):263 { 283, 1985.

[7] M. Colpi, S. L. Shapiro, and I. Wasserman. Boson stars: Gravitational equilibria of self-interacting scalar elds. *Phys. Rev. Lett.*, 57:2485{2488, Nov 1986.

[8] J. Ehlers and W. Kundt. Gravitation: An introduction to current research ed l witten, 1962.

[9] K. Enqvist, A. Jokinen, T. Multamaki, and I. Vilja. Constraints on self-interacting q-ball dark matter. *Physics Letters B*, 526(1):9{18, 2002.

[10] C. R. Evans and J. S. Coleman. Critical phenomena and self-similarity in the gravitational collapse of radiation uid. *Phys. Rev. Lett.*, 72:1782{1785, Mar 1994.

[11] R. Ferrell and M. Gleiser. Gravitational atoms: Gravitational radiation from excited boson stars. *Phys. Rev. D*, 40:2524{2531, Oct 1989.

[12] M. Gleiser and R. Watkins. Gravitational stability of scalar matter. *Nuclear Physics B*, 319(3):733 { 746, 1989.

[13] C. Gundlach. Critical phenomena in gravitational collapse. *Living Reviews in Relativity*, 2(1):4, 1999.

[14] S. H. Hawley and M. W. Choptuik. Boson stars driven to the brink of black hole formation. *Physical Review D*, 62(10):104024, 2000.

[15] T. Koike, T. Hara, and S. Adachi. Critical behavior in gravitational collapse of radiation uid: A renormalization group (linear perturbation) analysis. *Phys. Rev. Lett.*, 74:5170{5173, Jun 1995.

[16] A. Kusenko and P. J. Steinhardt. Q-ball candidates for self-interacting dark matter. *Physical review letters*, 87(14):141301, 2001.

[17] T. Lee and Y. Pang. Stability of mini-boson stars. *Nuclear Physics B*, 315(2):477 { 516, 1989.

[18] T. Lee and Y. Pang. Nontopological solitons. *Physics Reports*, 221(5):251 { 350, 1992.

[19] S. L. Liebling and C. Palenzuela. Dynamical boson stars. *Living Reviews in Relativity*, 15(1):6, 2012.

[20] C. F. Macedo, P. Pani, V. Cardoso, and L. C. Crispino. Astrophysical signatures of boson stars: quasinormal modes and inspiral resonances. *Physical Review D*, 88(6):064046, 2013.

[21] N. Manton and P. Sutcli e. *Topological solitons*. Cambridge University Press, 2004.

[22] E. W. Mielke and F. E. Schunck. Boson stars: Early history and recent prospects. *arXiv preprint gr-qc/9801063*, 1998.

[23] T. Multamaki and I. Vilja. Limits on q-ball size due to gravity. *Physics Letters B*, 542(1):137{146, 2002.

[24] F. Pretorius and R. Price. Project 2: Gravitational collapse in the spherically symmetric einstein-klein-gordon system. http://physics.princeton.edu/~fpretori/group_resources/ss_ekg/project_2.pdf. Accessed: 2017-05-08.

[25] R. Ru ni and S. Bonazzola. Systems of self-gravitating particles in general relativity and the concept of an equation of state. *Phys. Rev.*, 187:1767{1783, Nov 1969.

[26] F. E. Schunck and E. W. Mielke. General relativistic boson stars. *Classical and Quantum Gravity*, 20(20):R301, 2003.

[27] E. Seidel and W.-M. Suen. Dynamical evolution of boson stars: Perturbing the ground state. *Phys. Rev. D*, 42:384{403, Jul 1990.

[28] Y. Verbin. Solitonic and non-solitonic q-stars. *arXiv preprint arXiv:0708.2673*, 2007.

[29] N. Yunes, K. Yagi, and F. Pretorius. Theoretical physics implications of the binary black-hole mergers gw150914 and gw151226. *Physical Review D*, 94(8):084002, 2016.